SEDIMENTOLOGY the journal of the International Association of Sedimentologists

Sedimentology (2018) **65**, 2088–2116 doi: 10.1111/sed.12458

Recent morphology and sedimentary processes along the western slope of Great Bahama Bank (Bahamas)

MELANIE PRINCIPAUD*, THIERRY MULDER*, VINCENT HANQUIEZ*, EMMANUELLE DUCASSOU*, GREGOR P. EBERLI†, LUDIVINE CHABAUD* and JEAN BORGOMANO‡

**UMR 5805 EPOC, Université de Bordeaux, Allée Geoffroy St Hilaire, Pessac 33615, France (E-mail: melanie.principaud@u-bordeaux.fr)*

†Center for Carbonate Research, University of Miami, 4600 Rickenbacker Causeway, Miami, FL 33149, USA

‡Europôle Méditerranéen de l'Arbois, Université de Provence, Avenue Louis Philibert - BP 80, Aix en Provence Cedex 04 13545, France

Associate Editor – John Reijmer

ABSTRACT

Carbonate slopes and associated resedimented deposits have recently gained renewed interest because they represent volumetrically significant parts of carbonate platforms. Carbonate slopes are highly variable compositionally, architecturally and spatially due to a spectrum of sediment sources, resedimentation processes and controlling factors. Here, new high resolution acoustic data (including EM302 multi-beam echo-sounder and very high resolution seismic) and piston cores document highly diverse and complex morphological features along the north-western slope of Great Bahama Bank. The recent morphology of the slope is the result of the interplay between depositional and erosive processes that vary through time and along strike. The different sedimentary processes are recorded as a Pleistocene lowstand surface, characterized by many erosional features and a Holocene sedimentary wedge along the upper to middle slope that partially covers the underlying Pleistocene surface. Sedimentary processes during the Holocene are dominated by density cascading flows, which export muddy aragonitic sediment from the platform top towards the slope. Sedimentation rates, however, vary along strike due to platform top morphology combined with the variable strength of the basinal current. Reefs and islands in the Bimini area block off-bank sediment export, and shoals and tidal deltas from Cat Cay to the south reduce the density cascading processes. Numerous small and large slope failure scars show the instability of the steep slopes of Great Bahama Bank. Bottom currents dominate the lower slope and the basin. Striations and moats are the morphological expressions of current directions, while areas of non-deposition document strong current and concomitant removal of off-bank transported sediment along parts of the slope, while the Santaren Drift and the drift on the north-western edge of Great Bahama Bank act as the depositional locus for the fine-grained sediments transported in the current.

Keywords Carbonate slope, echo character, Great Bahama Bank, sea floor morphology, sedimentary processes, seismic facies.

 © 2018 The Authors. Sedimentology © 2018 International Association of Sedimentologists

INTRODUCTION

Great Bahama Bank (GBB) is the largest shallow-water carbonate platform of the Bahamian archipelago, which forms an extensive carbonate province in the western part of the North Atlantic. It is a modern example of an isolated carbonate platform that has been operating under tropical conditions as a highly productive carbonate factory since its inception in the Upper Jurassic (Purdy, 1963a,b; Schlager & Ginsburg, 1981; Masaferro & Eberli, 1999).

The GBB platform has concaved steepened flanks, typical of modern carbonate slopes (Adams & Schlager, 2000). Its western side corresponds to a leeward open margin (Hine *et al.*, 1981) typified by Quaternary accretionary slope development (Schlager & Ginsburg, 1981). The leeward margin is interrupted by the Bimini Island chain extending over 35 km and is prolonged by the presence of the Cat Cay Shoal and tidal deltas which represent the only well-developed shoals on this margin (Fig. 1). This ensemble forms a continuous to semi-continuous barrier over *ca* 80 km. This margin's physiographic variation could affect off-bank export and sedimentary distribution along the slope, thereby shaping the architectural elements of the slope. Moreover, ocean currents flowing in the Florida Straits and the Santaren Channel have influenced sedimentation and facies distribution along the western slope of GBB and in the basin (Fig. 1; Anselmetti *et al.*, 2000; Betzler *et al.*, 2014).

Several studies have focused on internal stratigraphic architecture and slope to basin evolution during the Neogene (e.g. Schlager & Ginsburg, 1981; Austin *et al.*, 1986; Eberli & Ginsburg, 1987, 1988, 1989; Ladd & Sheridan, 1987; Eberli *et al.*, 1997; Betzler *et al.*, 1999; Anselmetti *et al.*, 2000; Ginsburg, 2001; Bergman, 2005; Principaud *et al.*, 2017). The present study is based on a combination of subsea data that provide a large-scale view of the sedimentary distribution, something that is difficult to recognize if only using sedimentary data.

The CARAMBAR oceanographic cruise (2010; Mulder *et al.*, 2012) was the first to image a large portion (*ca* 180 × 50 km) of the Florida Straits adjacent to the north-western slope of GBB using modern high-quality multi-beam and extensive very high resolution seismic data (Chirp). These surveys revealed longitudinal morphological changes and several unexpected large-scale and small-scale morphologies occurring in variety of sedimentary environments (Mulder *et al.*, 2012). This study provides new valuable data on the morphology of GBB slopes and illustrates, for the very first time, the hydrodynamic processes that result in a range of slope to basin morphological features, sedimentary facies belt and slope architectural elements along a modern leeward carbonate slope. It represents a first step towards revision of early models of carbonate slope facies environments.

REGIONAL SETTING

Geological setting

The present-day platform morphology of GBB is the result of the complex tectonic and architectural evolution of the Bahamian archipelago since Early to Middle Jurassic rifting (Eberli & Ginsburg, 1987, 1989; Ladd & Sheridan, 1987; Denny *et al.*, 1994; Masaferro & Eberli, 1999). Bordered by the Atlantic Ocean and intersected by several deep channels (i.e. Providence Channel, Florida Straits, Santaren Channel, Old Bahama Channel), GBB is a pure carbonate province with no direct significant terrigenous input (Carew & Mylroie, 1997) besides windblown dust (Shinn *et al.*, 1989; Swart *et al.*, 2014). The Bahamas–Florida region has been tectonically stable since the Middle Tertiary, with a later period of lower shortening associated with the late part of the collision between Cuba and the Bahamas which is recorded in fold growth strata in the outer edges of the Cuban fold and thrust belt (Masaferro *et al.*, 2002). The north-western side of GBB currently consists of an open leeward margin, which has prograded in places up to 27 km towards the Florida Straits since the Middle Miocene (Eberli & Ginsburg, 1987, 1989).

The GBB is a flat-topped carbonate platform with an average water depth of 10 m and an area of *ca* 100 000 km^2 (Purdy, 1963a; Traverse & Ginsburg, 1966; Enos, 1974; Boss & Rasmussen, 1995; Reijmer *et al.*, 2009; Swart *et al.*, 2009; Harris *et al.*, 2015). The platform margin is a gently dipping surface from the platform interior to the platform edge and is up to 4 km wide. This margin is covered by skeletal carbonate sand of various thickness on a cemented platform top (Enos, 1974; Wilber *et al.*, 1990). At the platform edge, which is around 30 m water depth, the slope angle increases significantly from a few degrees to a very steep cliff (up to 45°) about 100 m in height (Wilber *et al.*, 1990; Wunsch *et al.*, 2016). The base of the cliff is characterized by an up to 300 m

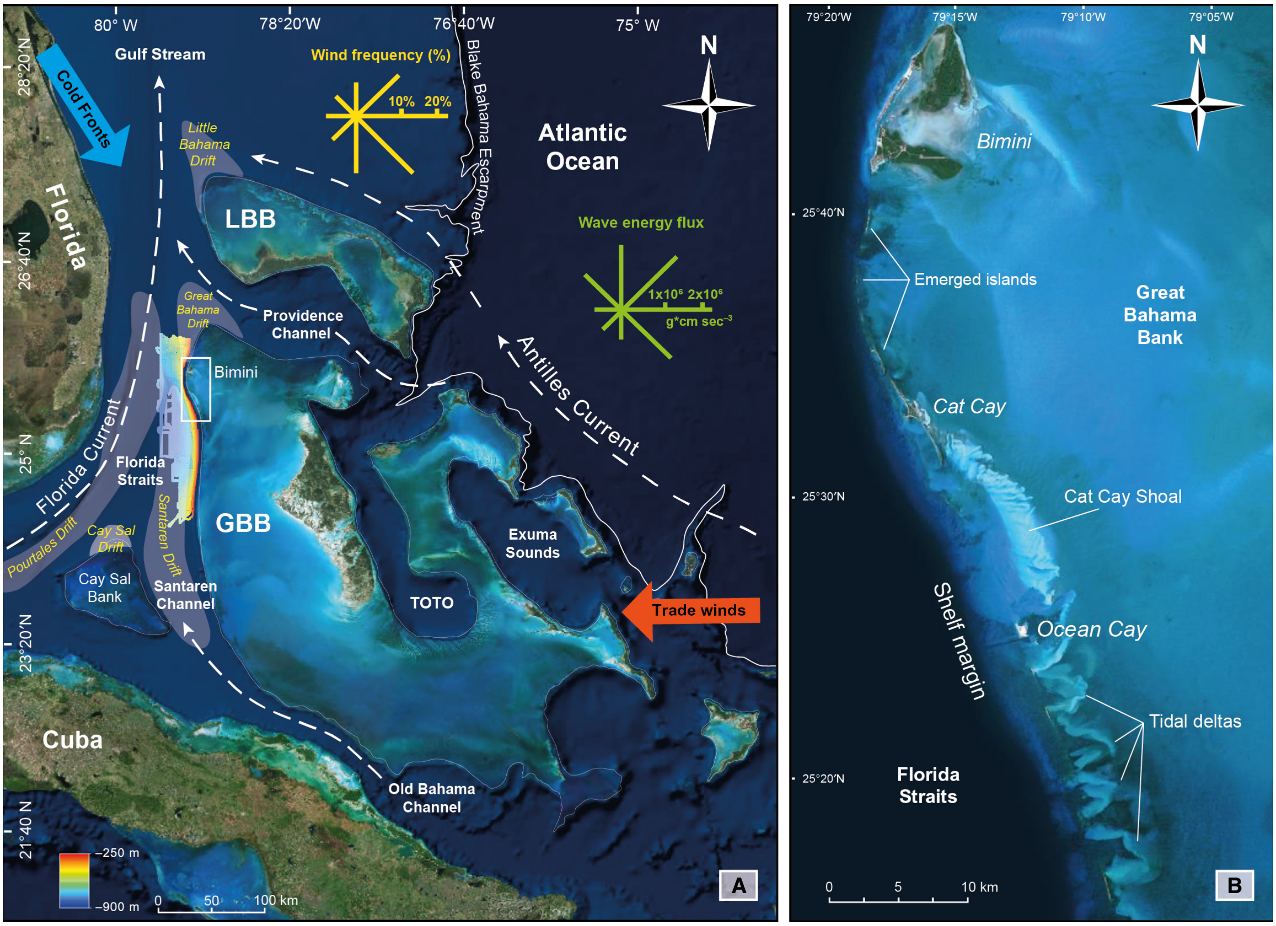

Fig. 1. (A) Regional setting of the Bahamas, showing the bathymetry of the study area along the north-western Great Bahama Bank (GBB) slope. The trajectories of the main oceanic currents in the Bahamian Archipelago are represented by white dashed arrows, and locations of the contourite drifts along the Florida Straits are marked by grey zones. Wind frequency and wave energy flux are also indicated (from Hine & Neumann, 1977). (B) Close-up of the Bimini area, including Bimini Islands, Cat Cay Shoal and tidal deltas southward. LBB, Little Bahama Bank.

wide and partially greater than 35 m deep margin-parallel depression described by Wilber *et al.* (1990, 1993) as an erosional trough, similar to a plunge pool. The slope angle decreases and gives way to a steep (*ca* 20°) cemented slope (Eberli *et al.*, 2004; Wunsch *et al.*, 2016). At about 160 m water depth the slope is onlapped by a soft sediment wedge defined as a ‘Holocene wedge’ (Wilber *et al.*, 1990; Roth & Reijmer, 2004, 2005) or ‘Holocene highstand wedge’ (Schlager *et al.*, 1994) that forms a gentle slope (2 to 8°) from 250 to 850 m water depth (Wilber *et al.*, 1990; Betzler *et al.*, 1999, 2014; Jo *et al.*, 2015).

Climate and oceanography

The present-day climate of the northern Bahamas is tropical to humid subtropical (Isemer & Hasse, 1985) and is influenced by strong trade winds (5 m sec^{-1}) throughout the year (Sealey, 1994; Rankey & Reeder, 2011). The easterly winds (from north-east, east and south-east) account for 77% of the wind frequency in August but only for 46% in February when cold north-westerly winds also occur (30%) (Bergman *et al.*, 2010). The north-westerly winds are often related to advancing cold fronts from the North American continent and pass over the archipelago from the north-west to the south-east (Fig. 1) (Roberts *et al.*, 1982; Sealey, 1994). Besides these winds, seasonal storms and tropical cyclones affect the archipelago. Despite the high wind speeds, waves only play a minor role in the sediment distribution of the platform-interior. Marginal islands and reefs attenuate large open ocean waves, reducing platform-interior waves to *ca* 1 m wave height (Rankey & Reeder, 2010). Consequently, on the platform top of the GBB the high-energy environments result from tidal currents accumulating large carbonate sand bodies (Ball, 1967; Purkis *et al.*, 2014). Wind-induced surface currents are mostly responsible for the distribution of fine sediments and the prevailing off-bank transport to the western leeward side of the banks (Eberli & Ginsburg, 1987; Wilber *et al.*, 1990; Milliman *et al.*, 1993; Roth & Reijmer, 2004, 2005). Tropical storms also sweep off mostly fine-grained carbonate particles from GBB (Wilber *et al.*, 1990; Wilson & Roberts, 1992; Eberli *et al.*, 1997; Swart *et al.*, 2000; Rendle & Reijmer, 2002; Roth & Reijmer, 2004, 2005; Rendle-Buehring & Reijmer, 2005). Cold fronts play an important role in off-bank transport along the margin; the cold front chills the water on the platform that is slightly elevated in salinity compared to the open ocean water (Wilson & Roberts, 1992, 1995). Chilling produces dense cold water that flows off the bank. Likewise, heavy evaporation during the summer heat can also increase the density of the water to produce an off-bank flow. This process is called density cascading (Wilson & Roberts, 1992, 1995; Wilber *et al.*, 1993). These downslope currents supply bank-derived particles to the along-slope-flowing ocean currents (Fig. 1).

The Florida Current is an energetic surface current that flows northward through the Florida Straits towards the North Atlantic and contributes 90% of the Gulf Stream (Mullins *et al.*, 1987; Leaman *et al.*, 1995; Lee *et al.*, 1995; Wang & Mooers, 1997). The Florida Current is mainly nourished by the outflow of the Loop Current of the Gulf of Mexico, with contributions of inflow from a weaker shallow current through the Santaren Channel (Atkinson *et al.*, 1995; Leaman *et al.*, 1995). The Florida and Santaren currents influence sea floor deposits and give rise to several contourite drifts in the Florida Bahamas region (Fig. 1), from south to north: Santaren Drift, Pourtales Drift, Cay Sal Drift, Great Bahama Drift and Little Bahama Drift (Mullins *et al.*, 1980; Bergman, 2005; Chabaud *et al.*, 2016; Principaud *et al.*, 2017). At depth, countercurrents and tidally driven reversing currents occur in the Florida Straits (Correa *et al.*, 2012a,b; Lüdmann *et al.*, 2016). Contour currents are important on the slope and the slope to basin transition because they can winnow and rework slope deposits, or prevent accumulation, resulting in periods of non-deposition (Coniglio & Dix, 1992; Kenter *et al.*, 2001; Rendle & Reijmer, 2002).

DATA AND METHODS

During the CARAMBAR cruise, carried out aboard the *R/V Le Suroît* in November 2010, continuous bathymetric and acoustic imagery data were collected using a Kongsberg EM302 multi-beam echo-sounder (Kongsberg Maritime AS, Kongsberg, Norway) (Mulder *et al.*, 2012). Bathymetric data were processed with Caraïbes software (Ifremer, Issy-les-Moulineaux, France) and meshed with a spatial resolution of 20 m (Fig. 2). Acoustic imagery data were processed with SonarScope software (Ifremer) and meshed with a spatial resolution of 5 m (Fig. 2). The multi-beam backscatter data were used to characterize the distribution of sedimentary facies along the slope. Changes in the backscatter values correspond to variations of the nature, the texture and the state of sediments and/or the sea-bed morphology (Unterseh, 1999; Hanquiez *et al.*, 2007). The 3·5 kHz sub-bottom profiler (Chirp mode) data were used to analyse the near-surface deposits. Classification and distribution of 3·5 kHz echo-facies are based on: (i) acoustic penetration and continuity of bottom and sub-bottom reflection horizons; (ii) micro-topography of the sea floor; and (iii) internal structures. Furthermore, studies in siliciclastic (Damuth & Hayes, 1977; Damuth, 1980) and carbonate environments (Mullins & Neumann, 1979; Mullins *et al.*, 1984) linking echo-facies and lithology provide a basis for interpreting these echo facies in terms of depositional environment. Finally, the top (10 cm) of 17 Kullenberg cores (Fig. 2B; Table 1) was used to calibrate the acoustic facies with the lithology, its composition and grain-size, and enabled better understanding of active sedimentary processes along the slope. For technical reasons, only soft sediments were sampled. Grain-size was measured using a Malvern Mastersizer S laser diffractometer (Malvern Instruments Limited, Malvern, UK) with the Fraunhofer method. Holocene sediments were identified in each core based on the occurrence of the planktonic foraminifera *Globorotalia menardii* complex (biozone Z; Ericson & Wollin, 1956; Ericson *et al.*, 1961). The last increase in *G. menardii* complex abundance has been dated at *ca* 11 ka cal BP on the Bahamas slopes (Ducassou *et al.*, 2014; Chabaud, 2016). This age has been used to calculate sedimentation rates in this study.

© 2018 The Authors. Sedimentology © 2018 International Association of Sedimentologists,

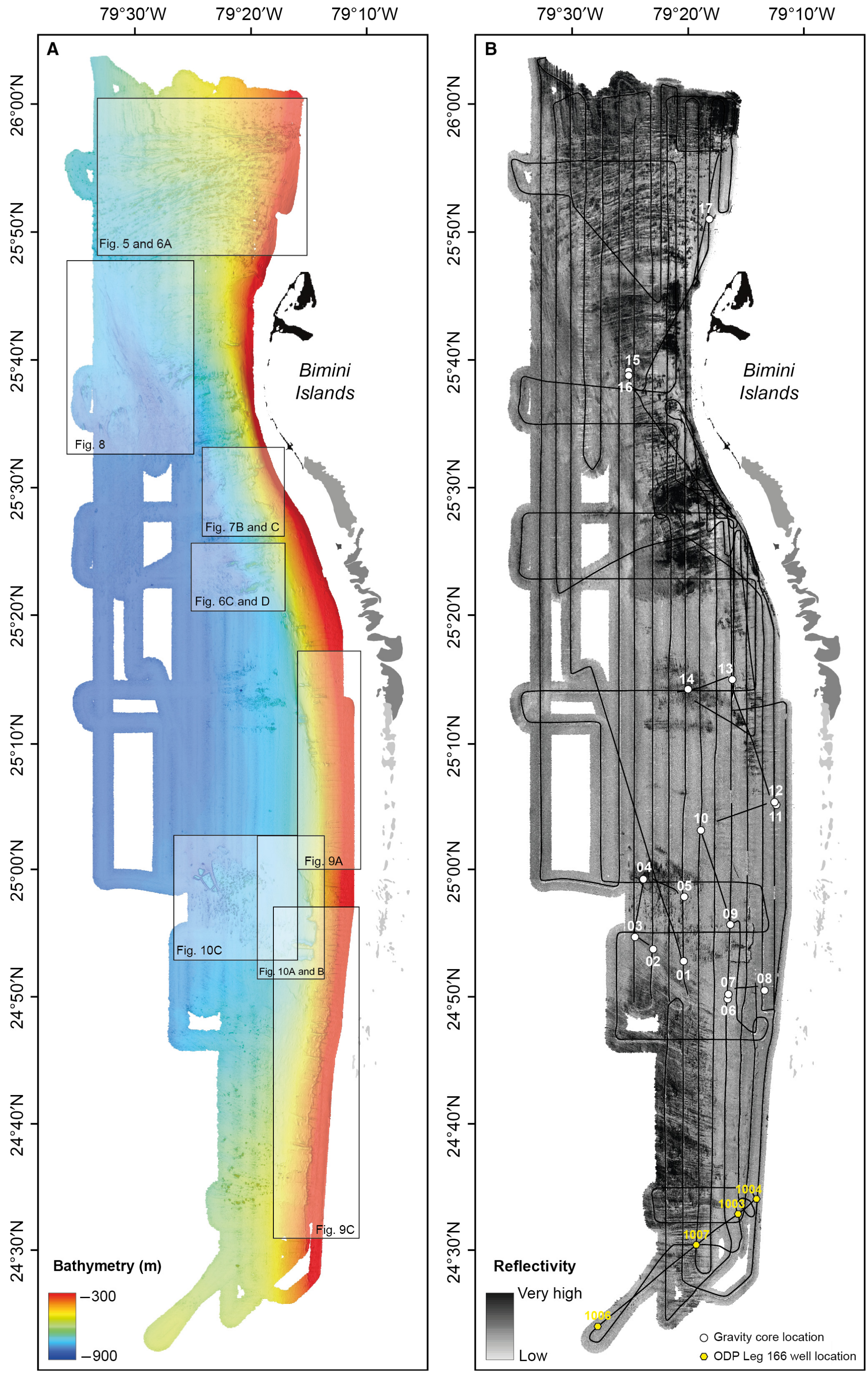

Fig. 2. (A) High resolution EM302 bathymetric map of the study area (CARAMBAR cruise). (B) High resolution EM302 acoustic imagery map of the study area (CARAMBAR cruise). Black lines correspond to very high resolution (Chirp) seismic profiles. White numbers are core locations.

Table 1. Core characteristics; core location shown in Fig. 2: CARKS – CARambar Kullenberg Sample.

Core	Latitude N	Longitude W	Depth (m)	Length (m)
CARKS-01	24°52′956	79°20′469	804	3·69
CARKS-02	24°53′885	79°23′094	812	3·61
CARKS-03	24°54′847	79°24′698	836	3·62
CARKS-04	24°59′368	79°23′948	829	2·11
CARKS-05	24°58′029	79°20′441	815	6·52
CARKS-06	24°49′977	79°16′659	731	7·27
CARKS-07	24°50′328	79°16′603	723	7·28
CARKS-08	24°50′657	79°13′482	488	7·18
CARKS-09	24°55′823	79°16′415	788	8·86
CARKS-10	25°03′242	79°18′985	824	7·25
CARKS-11	25°05′290	79°12′469	449	3·68
CARKS-12	25°05′481	79°12′612	456	8·51
CARKS-13	25°15′109	79°16′281	722	9·95
CARKS-14	25°14′032	79°20′924	828	7·88
CARKS-15	25°38′709	79°25′164	770	6·03
CARKS-16	25°38′399	79°25′152	807	3·26
CARKS-17	25°51′189	79°18′270	425	11·53

RESULTS

Slope morphology and depositional setting of the Great Bahama Bank

The general shape and configuration of the slope is illustrated in Fig. 3. The slope is subdivided into four domains.

1 The upper slope consists of the lower part of the cemented slope and the upper portion of the soft sediment wedge and extends to a water depth of *ca* 350 m. The water depth at which the cemented and uncemented slope occurs, however, is highly variable.

2 The middle slope extends to 600 m water depth. Its slope angle varies between 2·0° and 7·5°. It shows furrows and failure scars in the northern area and an extended gully system partly intersected by a large escarpment in the southern area (Figs 2 and 3).

3 The lower slope extends between 600 m and 850 m of water depth with a slope angle ranging between 0·4° and 2·0°. This domain is generally characterized by bypass and/or erosion areas as indicated by numerous furrows and failure scars. The central part of the study area shows a large mass transport complex (MTC; Principaud *et al.*, 2015) (Figs 2 and 3) whose blocks and boulders serve as the foundation for numerous cold-water coral mounds (Correa *et al.*, 2012b; Sianipar, 2013; Lüdmann *et al.*, 2016).

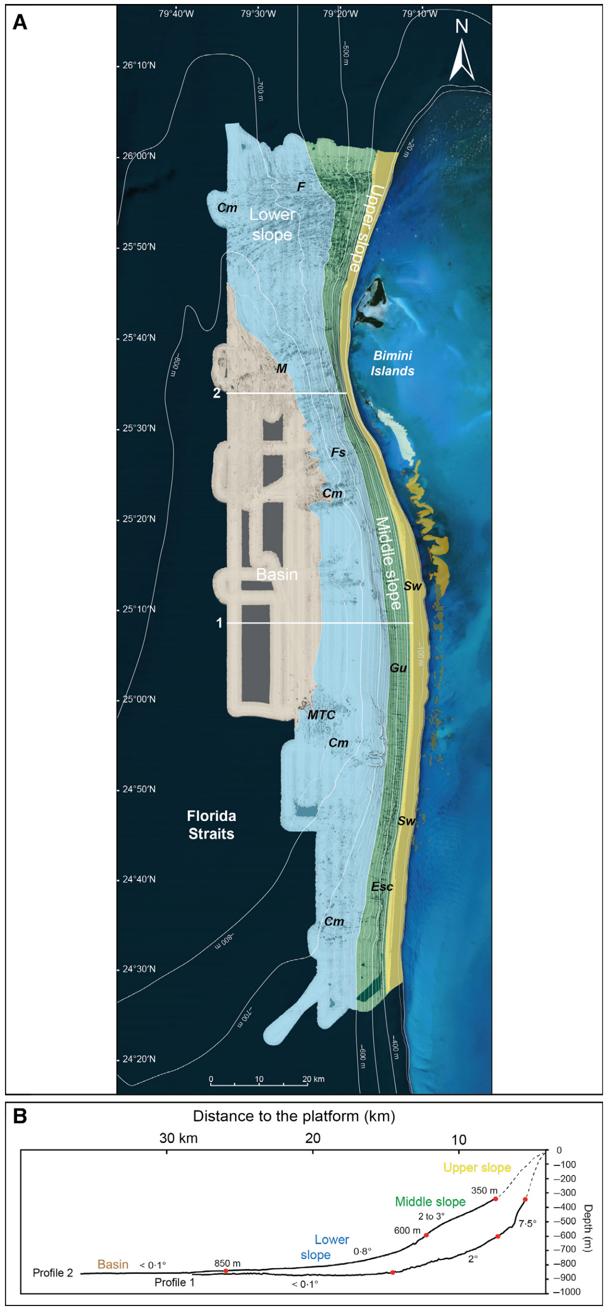

Fig. 3. (A) Map of the study area showing physiographic domains of the slope. (B) Slope profile (vertical exaggeration x12); hatched area provided from NOAA bathymetric data. Bl, Blocs; Cm, Carbonate coral mounds; Esc, Escarpment; F, Furrows; Fs, Failure scars; Gu, Gullies; M, Moat; MTC, Mass Transport Complex; Sc, Scars; Sw, Sediment waves.

4 The basin extends beyond 850 m water depth with a <1° dipping slope. It shows a well-developed moat and associated elongated current marks (Figs 2 and 3).

Slope profiles indicate a distinct morphology offshore Bimini Islands with a shorter and steeper slope with many erosional features compared to the area along strike where no shelf-edge barrier exist (Figs 2 and 3).

Acoustic facies

Ten acoustic facies have been identified based on backscatter value variations; they are divided into four classes (Table 2): (i) very high; (ii) high; (iii) medium; and (iv) low reflectivity. In addition, eight types of sedimentary structures were observed with either east–west (downslope) or north–south (along strike) orientations.

Low reflectivity acoustic facies are mainly associated with sedimentary bodies such as sediment waves (S-2; Fig. 4A) or are associated with carbonate coral mounds (S-3). In contrast, medium to high reflectivity acoustic facies tend to be associated with erosive sedimentary features (S-4, S-5 and S-7; Fig. 4A) such as furrows and comet-tail structures.

The very high reflectivity acoustic facies, both homogeneous and heterogeneous, are observed north of 25°25′N (Fig. 4A). The homogeneous acoustic facies A-I forms scattered patches along the middle and lower slopes. The heterogeneous acoustic facies A-II shows discontinuous and narrow bands (*ca* 10 km long/*ca* 3 km wide) along the middle and upper steepest slope west of Bimini Islands (Table 1; Fig. 4A).

Areas with high reflectivities form large slope parallel longitudinal bands (>50 km long and 6 to 20 km wide) which are restricted to the lower slope, (Table 2; Fig. 4A). The acoustic facies B-II.1 which appears heterogeneous with a mottled aspect is associated with erosional furrows with downslope orientation (S-4 and S-7; Table 2; Fig. 4A). This facies is observed north of 25°20′N and south of 25°55′N. The heterogeneous acoustic facies B-II.2 with chevron patterns is only present in the northernmost part of the study area along the lower and middle slopes. Acoustic heterogeneous facies B-II.3 and B-II.4 (heterogeneous with stripey aspect) are restricted to the median part of the study area (Fig. 4A). The acoustic facies B-II.3 forms a narrow longitudinal stripe (*ca* 38 km long and *ca* 3 km wide) along the middle slope and is generally associated with downslope-oriented, slightly erosive furrows (S-1 and S-8; Table 2; Fig. 4A). The acoustic facies B-II.4 forms scattered patches of about 75 to 150 km^2 on the lower slope and is associated with north–south-oriented erosive structures (S-5; Table 2; Fig. 4A).

Medium reflectivity facies are observed north of 25°N (Fig. 4A). The homogeneous acoustic facies C-I is observed in the basin where it is associated with slope parallel linear erosive structures (S-5; Table 2; Fig. 4A) and comet-tail structures (S-6; Table 2; Fig. 4A). The heterogeneous acoustic facies C-II is present along the upper slope and on the top of the middle slopes where it forms a continuous narrow band of 0·5 to 2·0 km that extends over *ca* 50 km west of Bimini (Fig. 4A).

Low reflectivity acoustic facies cover the largest surface of the study area (Fig. 4A). They cover a wide continuous area from the upper slope to the basin south of 25°25′N, while they are more scattered north of this latitude. The homogeneous acoustic facies D-I is continuous along the upper to middle slope. North-west of Bimini the facies is associated with sub-circular structures of very high reflectivity (S-3; Table 2; Fig. 4A), while it shows discontinuous patches along the middle slope, west of Bimini (Fig. 4A). In the median part of the study area, the acoustic facies D-I covers almost the entire slope (Fig. 4A). It is devoid of sedimentary structures in the lower slope and the basin, while it is associated with along-slope wavy linear structures (S-2; Table 2; Fig. 4A) and downslope linear structures (S-8; Table 2; Fig. 4A) along the upper to middle slopes. In the southern area, the acoustic facies D-I is continuous between the upper and the top of lower slope and is associated with along-slope undulating sedimentary structures (S-2; Table 2; Fig. 4A) and downslope linear structures (S-8; Table 2; Fig. 4A). Finally, the heterogeneous acoustic facies D-II is only observed along the lower slope (Fig. 4A).

Echo-facies

Eleven echo-facies have been identified and grouped into five main classes (Table 3): (i) bedded; (ii) hyperbolic; (iii) transparent; (iv) chaotic; and (v) combined echo-facies. Although a few transitions between echo-facies are sharp, most of them are gradual and characterized by combined echo-characters.

Bedded echo-facies are mainly present south of 25°25′N and show a downslope distribution (Fig. 4B; Table 3). Continuous bedded echo-facies (I-1) is only present in the basin. Discontinuous bedded echo-type (I-2) forms discontinuous patches along the middle slope, west of Bimini Islands, and passes upslope into an undulated

Table 2. EM302 acoustic facies classification.

Class	Type	Legend	EM302 detail	Description	Location
A. Very high reflectivity	A-I		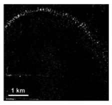	Homogeneous, without apparent structures	Patch distribution in the north area: (i) in the middle slope between −350 m and −475 m of water depth; and (ii) in the lower slope between −600 m and −850 m of water depth
	A-II		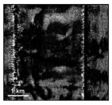	Heterogeneous, with black spotted aspect	Seaward*Bimini Islands*, in the middle slope, between −375 m and −600 m of water depth
B. High reflectivity	B-II.1		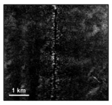	Heterogeneous, with mottled aspect	In the north, in the middle to lower slope, between −375 m and −650 m of water depth
	B-II.2		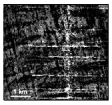	Heterogeneous, with chevron-patterned	Wide areas along the lower slope, between −640 m and −850 m of water depth
	B-II.3		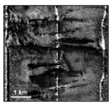	Heterogeneous	Patch distribution in the middle to lower slope, between −425 m and −700 m of water depth
	B-II.4		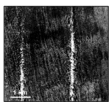	Heterogeneous, with stripey aspect	Patch distribution in the lower slope, between −775 m and −850 m of water depth
C. Medium reflectivity	C-I		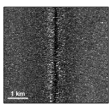	Homogeneous, without apparent structures	Lower slope to basin, below −780 m of water depth
	C-II		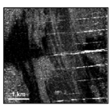	Heterogeneous with spots of variable reflectivity	Upper and middle slope, above −500 m of water depth
D. Low reflectivity	D-I		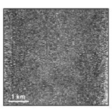	Homogeneous, without apparent structures	Upper slope to basin
	D-II		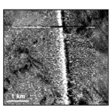	Heterogeneous with mottled aspect	Lower slope, between −625 m and −850 m of water depth
Sedimentary structures	S-1		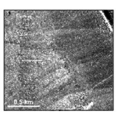	E–W linear converging structures	In the upper to middle slope, between −300 m and −570 m of water depth
	S-2		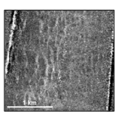	Along-slope wavy structures	In the half south part of the study area, in the upper to middle slope, between −320 m and −750 m of water depth

© 2018 The Authors. Sedimentology © 2018 International Association of Sedimentologists,

Table 2. (continued)

Class	Type	Legend	EM302 detail	Description	Location
	S-3		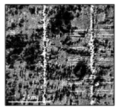	Sub-circular spots of very high reflectivity	Patch distribution in the north, in the middle slope, between −450 m and −620 m of water depth
	S-4		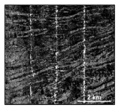	E−W distributary furrows	In the north, in the lower slope, between −490 m and −590 m of water depth
	S-5		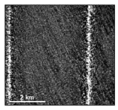	SE−NW linear structures	In the lower slope and in the basin, between −820 m and −870 m of water depth
	S-6		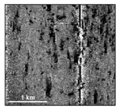	High reflectivity structures with N−S comet-tail	Patch distribution in the lower slope and the basin, between −800 m and −850 m of water depth
	S-7		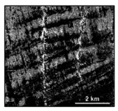	Subparallel linear furrows with E−W orientation	In the lower slope: (i) seaward Bimini Islands, between −700 m and −850 m of water depth; and (ii) in the south, between −620 m and −830 m of water depth
	S-8		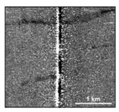	Subparallel sub linear structures with E−W orientation	Along the middle slope, between −420 m and −600 m of water depth

continuous bedded echo-facies (I-3). This echo-facies is observed along the upper to middle slope, north of Bimini Islands, and along the middle slope, south of 25°20′N, where it forms a *ca* 6 km wide and 110 km long, north–south oriented facies belt. Bedded echo-facies are commonly associated with hemipelagic sediments interbedded with gravity flow deposits (Damuth, 1979, 1980; Mullins *et al.*, 1984).

Hyperbolic echo-facies are mainly present north of 25°20′N (Table 3; Fig. 4B). Large, irregular hyperbolae (II-1) form 6 to 20 km wide stripes and >50 km long stripes along the lower slope. In the basin this echo-facies laterally passes to small and irregular hyperbolae (II-2). Formation of hyperbolae is mainly related to roughness of the sea floor topography. Large, irregular hyperbolae are generally associated with topographic edges related to failure scars and submarine or erosional topography whereas small regular hyperbolae are commonly associated with mass flow deposits (Damuth, 1980; Mullins *et al.*, 1984).

The transparent echo-facies (III-1) is present between 24°50′N and 25°05′N, along the lower slope and in the basin (Table 3; Fig. 4B). This echo-facies commonly corresponds to massive deposits. Its internal structure generally lacks distinct reflectors and appears to be acoustically transparent (Embley, 1976, 1980; Damuth, 1980, 1994) while its erosive base appears more reflective.

Chaotic echo-facies (IV-1) form a narrow north–south oriented stripe (*ca* 2 km wide and *ca* 100 km long), along the upper slope, south of 25°30′N (Table 3; Fig. 4B). This echo-facies, parallel to the echo type I-1, could correspond to highly disorganized sediments generally induced by mass-wasting processes such as slump deposits or debrites (Damuth, 1994).

Combined echo-facies are sparsely distributed over the study area and correspond to transitional facies (Table 3; Fig. 4B). The echo-facies V-1, observed along the middle slope, is characterized by high-amplitude hyperbolae draped by a low to transparent, discontinuous to

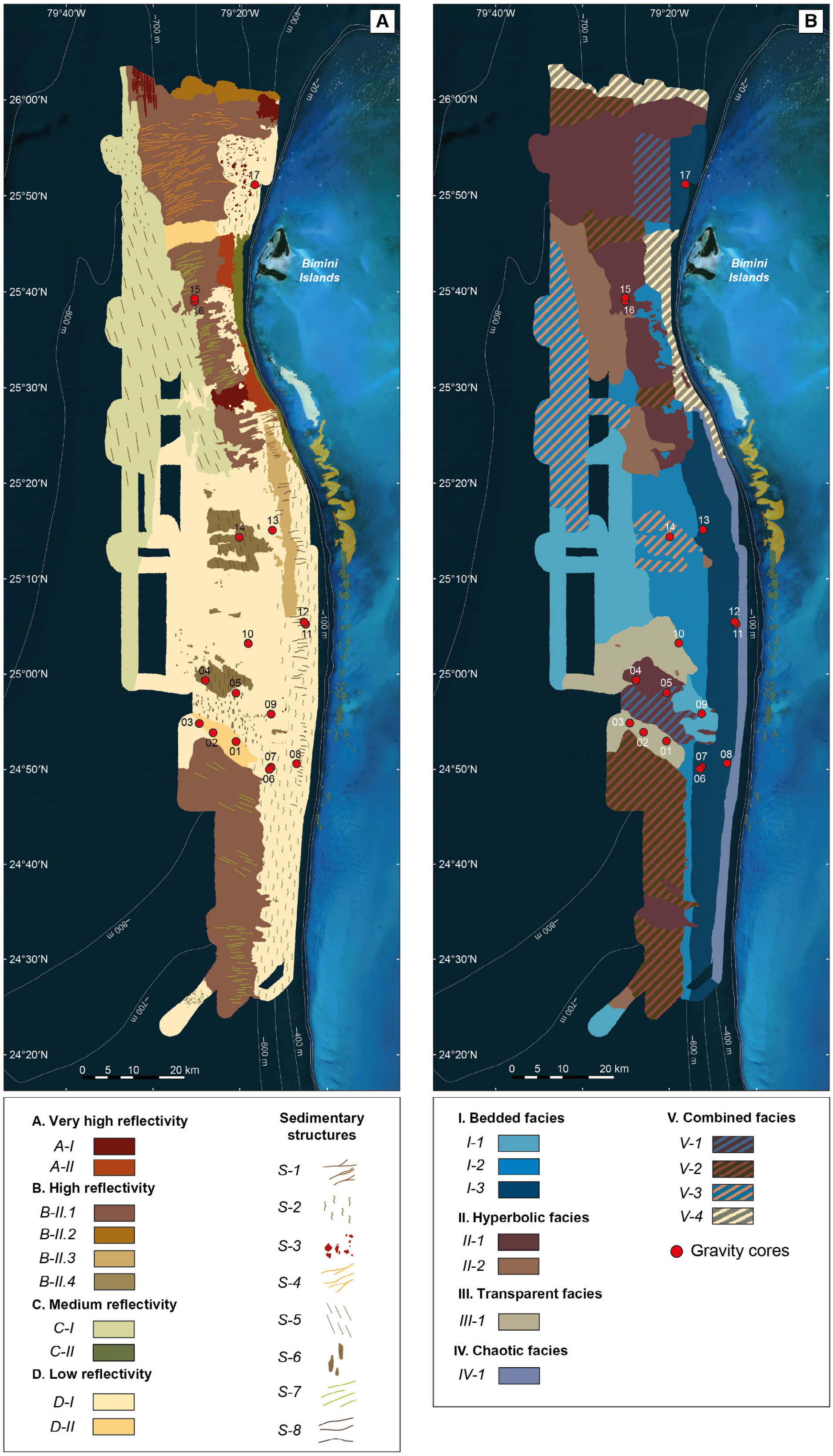

Fig. 4. (A) EM302 reflectivity map; and (B) echo-character map of the north-western Great Bahama Bank slope and adjacent Florida Straits.

© 2018 The Authors. Sedimentology © 2018 International Association of Sedimentologists, *Sedimentology*, **65**, 2088–2116

Table 3. Echo-character classification.

Class	Type	Legend	Chirp detail	Description	Location
I. Bedded	I-1		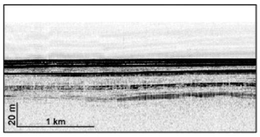	Bottom echo: high amplitude, sharp, planar and continuous Internal reflectors: numerous, distinct, continuous and parallel or subparallel to the sediment surface	Wide area in the basin beyond −850 m of water depth
	I-2		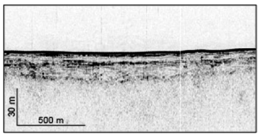	Bottom echo: high amplitude, sharp, planar and continuous Internal reflectors: numerous, discontinuous and parallel or sub-parallel to the sediment surface	Wide area in the lower slope, between −730 m and −850 m of water depth Patch distribution along the middle slope between −375 m and −750 m of water depth
	I-3		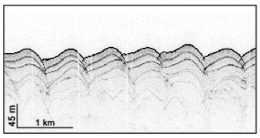	Bottom echo: sharp, undulated and continuous Internal reflectors: numerous, distinct, undulated, continuous and parallel or sub-parallel to the sediment surface	Along the middle slope, between −425 m and −725 m of water depth
II. Hyperbolic	II-1		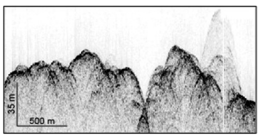	Bottom echo: large irregular overlapping hyperbolae of strong amplitude with varying vertex elevation above the sea floor Internal reflectors: none	Along the lower slope, generally between −600 m and −850 m of water depth, in the north Patchy distribution in the south, between −780 m and −860 m of water depth
	II-2		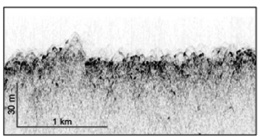	Bottom echo: numerous small irregular overlapping hyperbolae of low to moderate amplitude with varying vertex elevation above the sea floor Internal reflectors: none	In the north, along the lower slope, between −800 m and −860 m of water depth
III. Transparent	III-1		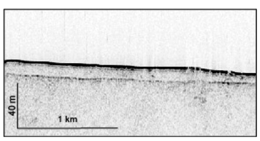	Bottom echo: sharp, high amplitude, prolonged and continuous Internal reflectors: acoustically transparent masses limited to the base by a continous to discontinuous reflector of moderate amplitude	Basinward areas distributed in the lower slope beyond −780 m of water depth

Table 3. (continued)

Class	Type	Legend	Chirp detail	Description	Location
IV. Chaotic	IV-1		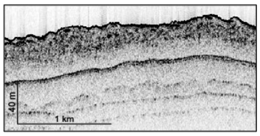	Bottom echo: sharp, high amplitude, undulated and continuous Internal reflectors: acoustically chaotic and indistinct masses of moderate amplitude covering distinct and continuous undulated internal reflectors parallel or subparallel to the sea floor	South of *Bimini Islands*, along the upper slope, above −430 m of water depth
V. Combined	V-1		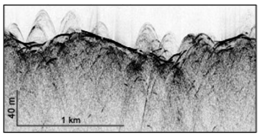	Bottom echo: numerous irregular overlapping hyperbolae with varying vertex elevation above the sea floor with discontinuous thin drape of layered reflectors with low to transparent amplitude Internal reflectors: none	Patch distribution in the lower slope: (i) in the north between −580 m and −680 m of water depth; and (ii) in the median part between −600 m and −850 m of water depth
	V-2		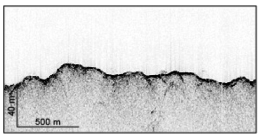	Bottom echo: sharp, continuous, high amplitude with some overlapping hyperbolae with vertices tangent to the sea floor Internal reflectors: none	Patch distribution of variable dimension, along the lower slope: (i) in the north, between −600 m and −850 m of water depth; and (ii) in the south between −625 m and −840 m of water depth
	V-3		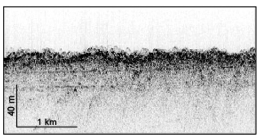	Bottom echo: numerous small overlapping hyperbolae of low to moderate amplitude with varying vertex elevation above the sea floor Internal reflectors: numerous, parallel or subparallel and discontinuous to the sediment surface	Wide areas in the lower slope and the basin, between −600 m and −850 m of water detph
	V-4		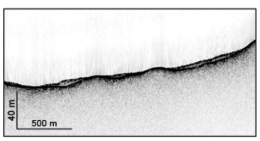	Bottom echo: sharp, high amplitude, prolonged and continuous, overcome by discontinuous lens of acoustically transparent masses	Along the upper slope, seaward *Bimini Islands*, above −600 m of water depth

continuous layered echo-facies corresponding to the superposition of echo-facies I-3 and II-1 (Table 3; Fig. 4B). The echo-facies V-2, observed along the lower slope, is characterized by a rough-appearing facies (irregularities are present) with very few small hyperbolae associated with echo-facies I-2. The echo-facies V-3, observed along the lower slope and the basin, is characterized by a discontinuous bedded echo-facies cut by small hyperbolae corresponding to the superposition of echo-facies I-2 and II-2 (Table 3; Fig. 4B). The echo-facies V-4, mainly present west of Bimini Islands, along the middle to upper slope, shows similarities with the III-1 transparent echo-facies, although transparent bodies are discontinuous and lenticular.

Grain-size and lithology of surface sediments

The grain-size distribution, the associated facies and the calculated average sedimentation rate during the Holocene (Table 4) are based on the analysis of the sediment core tops. Surface sediments sampled in the cores consist of a relatively homogeneous facies of silty mudstone to wackestone. Grain-size data reveal a bimodal distribution with a dominant silty mode along with a secondary mode at 10 μm that corresponds to mud (Table 4). This mud contains mainly aragonite needles derived from the platform and pelagic components (planktonic foraminifera and coccolithophoridae) (Chabaud *et al.*, 2016; Chabaud, 2016). Some cores (CARKS 05 and CARKS 10; CARKS, CARambar Kullenberg Sample) indicate coarser surface sediment corresponding to silty mud and sandy wackestone. The sand-sized fraction stems from planktonic foraminifera and pteropods coming from the water column (Chabaud *et al.*, 2016; Chabaud, 2016).

Sediment cores sampled in topographic depressions such as CARKS 06 (filling of a buried channel-levée complex; Mulder *et al.*, 2014), CARKS 09 (filling of the MTC escarpment) and CARKS 14 (filling of a pockmark) are predominantly muddy (Table 4). Coarser sediments (CARKS 05 and CARKS 10) are more abundant along the lower slope, further away from the platform. The lack of mud in this area is probably due to the winnowing of mud by the Santaren Current (Betzler *et al.*, 2014).

Holocene sedimentation rates display an east–west gradient along the slope. The northern area (CARKS 17) has the highest sedimentation rates around 140 cm ka^{-1}. High rates are also found in topographic depressions (CARKS 06). The rest of the area shows sedimentation rates around 30 cm ka^{-1} along the middle slope, which significantly increase at the gully system base (40 to 50 cm ka^{-1}) and reduce towards the lower slope and the basin (1 to 2 cm ka^{-1}).

INTERPRETATION AND DISCUSSION

The detailed maps using bathymetry, acoustic facies and echo-facies show a downslope facies distribution characterized by large, slope parallel longitudinal bands associated with specific morphological features that accurately depict the interplay of different sedimentary processes (off-bank transport, along-slope transport and erosion) along the leeward margin of GBB.

Diversity of morphological features along the slope

The erosional surface

In the northern area, the middle to lower slope shows a very irregular surface characterized by high reflectivity acoustic facies (B-II.1) associated with hyperbolic echo-facies (II-1) (Fig. 4). This particular surface corresponds to lithified or coarse-grained deposits and is crossed by a complex anastomosing network of discontinuous erosional furrows perpendicular to the platform margin (S-4) (Figs 2, 5, 6A and 6B). These erosional channels are located along the middle to lower slope and they bend southward in the lower slope. They show a V-shape symmetrical morphology, 2·5 to 6·0 km long, 150 to 300 m wide, and 5 to 20 m deep. Several-metre-high ridges separate these downslope grooves. The hardground surface with alternating ridges and grooves is responsible for the hyperbolic echo-facies (II-1) (Fig. 5). The central part of the grooves shows low reflectivity, indicating a partial filling with soft fine-grained sediments (Figs 5 and 6B). Abundant cold-water coral mounds (S-3) grow on the ridges with a preferentially downslope orientation (Fig. 6) and have varying sizes of a few metres to several tens of metres in diameter and height (Correa *et al.*, 2012b). Many of the hyperbolic echo-facies are also boulders and blocks that litter the slope; they can act as the starting point of cold-water coral accumulations consisting mainly of scleractinian branching corals associations (*Lophelia pertusa* and *Enallopsammia profonda*) (Hebbeln *et al.*, 2012). These are very abundant between 250 m and 850 m water depth and preferentially settled and aligned on topographic highs (furrow ridges and blocks) mostly along ridges perpendicular to the bank margin (Lüdmann *et al.*, 2016).

The Holocene depositional wedge and its lateral variability

The leeward margin of GBB shows a thinning-downslope sedimentary wedge, which is characterized by the presence of low reflectivity acoustic facies (D-1) generally, associated with bedded echo-facies along most of the upper to middle slope. In the northern area, the sedimentary wedge covers the previous furrow surface.

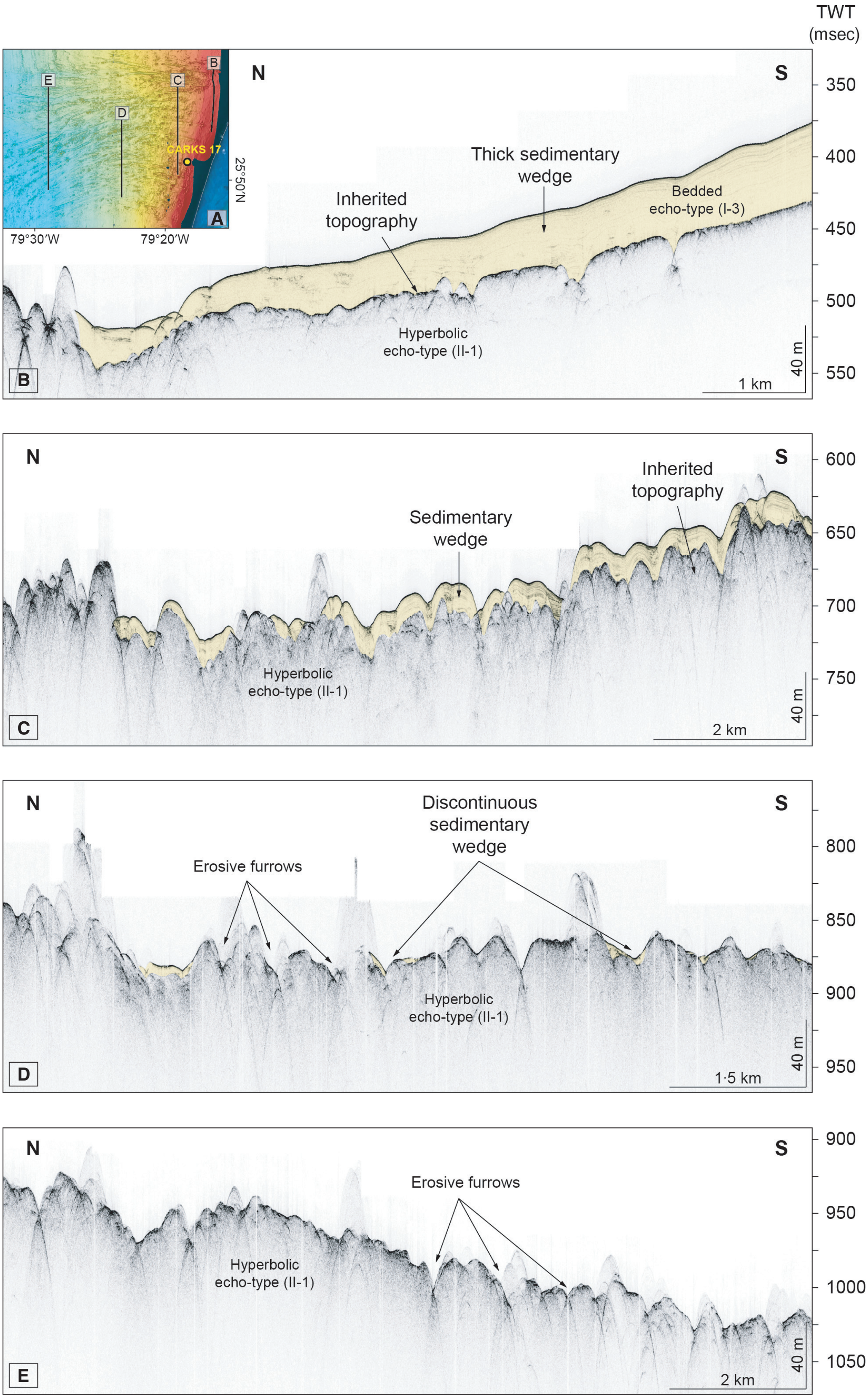

Fig. 5. Chirp profiles of the northern area showing the east–west extension of the Holocene sedimentary wedge which covers erosional furrows.

Table 4. Depositional environment, major grain-size classes and distribution of surficial sediments and Holocene sedimentation rates.

Core	Depositional environment	Grain size (%) Clay-size (<10 μm)	Silt	Sand	Granulometric distribution	Facies (Chabaud, 2016)	Holocene thickness (cm)	Holocene sedimentation rate (cm ka^{-1})
CARKS-01	Lower slope	30·8	39·8	29·3		Silty mud wackestone	25	2·3
CARKS-02	Lower slope	41·7	33·8	24·4		Silty mud wackestone	15	1·4
CARKS-03	Lower slope	34·8	38·4	26·8		Silty mud wackestone	12	1·1
CARKS-04	Lower slope – Carbonate block	32·5	42·1	25·3		Silty mud wackestone	*	*
CARKS-05	Lower slope – Mass Transport Deposit	26·5	32·3	41·2		Silty mud to sandy wackestone	*	*
CARKS-06	Lower slope – Filling of channel -levée complex	43·3	50·1	6·5		Silty mud wackestone	573	163·7
CARKS-07	Lower slope – Channel-levée complex	25·9	67·7	6·4		Silty mud wackestone	480	43·6
CARKS-08	Middle slope – Gully system	43·3	45·9	10·8		Silty mud wackestone	625	61·3
CARKS-09	Lower slope	45·7	48	6·2		Silty mud wackestone	540	49·1
CARKS-10	Lower slope	23·8	29·2	46·9		Silty mud to sandy wackestone	*	*
CARKS-11	Middle slope – Gully system	36·9	48·2	14·8		Silty mud wackestone	320	29·1
CARKS-12	Middle slope – Gully system	31·0	35·5	33·5		Silty mud wackestone	170	15·5
CARKS-13	Lower slope	28·3	50·3	21·3		Silty mud wackestone	180	16·4
CARKS-14	Lower slope – Pockmark	62·7	35·7	1·5		Muddy wackestone	480	34·3
CARKS-17	Middle slope – Sedimentary wedge	26·3	49·6	24		Silty mud wackestone	1030	137·3

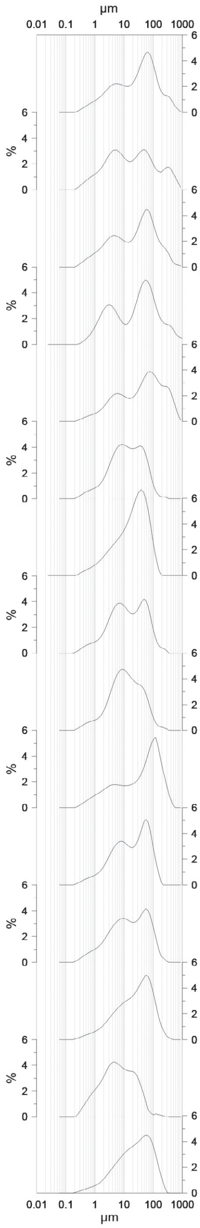

*Absence of Holocene sediment or, reworked sediment. CARKS, CARambar Kullenberg Sample.

It forms a 0 to 50 m thick wedge of low reflectivity acoustic facies (D-1) associated with bedded (I-3) and combined echo-facies (V-1) and ends at the lower slope transition (Figs 4 and 5). South of Bimini Islands this low acoustic facies is also present along the upper to middle slope, associated with chaotic (IV-1) and bedded (I-3) echo-facies (Fig. 4). However, this same portion of the

© 2018 The Authors. Sedimentology © 2018 International Association of Sedimentologists,

slope along Bimini Islands is characterized by an alternation of layers with contrasting reflectivity (A-II and C-II), indicating locally a strong sediment and/or cementation heterogeneity (Fig. 4A). The associated echo-type IV-4 (Fig. 4B) shows an irregular and rugged surface made of depressions which are filled by thin lenses of transparent facies (Fig. 7).

This low acoustic facies, present along most of the upper to middle slope, corresponds to unconsolidated silty mud wackestone (Table 4) and forms a sedimentary wedge commonly referred to as the 'Holocene wedge' (Wilber *et al.*, 1990; Schlager *et al.*, 1994; Roth & Reijmer, 2004, 2005). It is also found along the uppermost slope of the Little Bahama Bank (Rankey & Doolittle, 2012; Mulder *et al.*, 2017). This thinning-downslope sedimentary wedge consists predominantly of aragonite mud-size particles derived from the bank since the late bank-top Holocene flooding (Wilber *et al.*, 1990). Roth & Reijmer (2004) dated the base of the wedge at 7·23 ka BP.

The thickness of the wedge along the bank margin greatly varies from north to south (Fig. 11). In the northern area, it is up to 50 m thick (Fig. 5) and shows the greatest sedimentation rates during the last 7·23 ka BP with an average of 140 cm ka^{-1} at 425 m water depth (Table 4; Fig. 11). This sedimentation rate is in concert with values (up to 13·8 m kyr^{-1}) reported higher on the slope by Roth & Reijmer (2004, 2005). South of Bimini Islands, the sedimentation rate of the wedge is around 15 to 30 cm ka^{-1} during the Holocene (Table 4; Fig. 11). From here to over 100 km south, the wedge is partly ornamented by sediment waves and dissected by shallow gullies. Between these two areas, the edge of the upper slope, the steepest part of the slope is cemented while thin lenses (<5 m thick) of unconsolidated, coarse bioclastic sediment, rich in green algae (*Halimeda* sp.) are deposited in the smoother downslope parts or in topographic depressions (Fig. 7) (Freile *et al.*, 1995). These lenses are limited to the platform edge and to the upper slope, indicating restricted sediment off-bank export during the Holocene (Wilber *et al.*, 1990). The irregular underlying surface would be the equivalent to the Pleistocene surface with erosional furrows described in the northern part of the study area (Fig. 7D).

This change of sedimentation rates is likely to be the combined product of different rates of off-bank export along the slope. It has been shown to occur mostly during the time when the platform is flooded, which occurs during the last 6 kyr of the Holocene.

Other shallow isolated carbonate banks like the Pedro Bank (Northern Nicaragua Rise) and the southern shelf of Jamaica reveal the existence of well-defined 20 to 50 m thick Holocene sediment wedges of bank-derived sediments on the upper and middle slopes (Glaser & Droxler, 1991). Sedimentation rates for the past 2500 years range between 2000 mm kyr^{-1} off Pedro Bank to 1200 mm kyr^{-1} off the southern Jamaica shelf (Glaser & Droxler, 1991) which are consistent with those observed during the Holocene along the GBB slope.

The steepened slope of Bimini with incipient failures

The median area located along Bimini Islands corresponds to the shortest and steepest slopes of the study area. Evidence for slope instabilities and erosional features is widespread along this part of the slope and characterized by a large band of high reflectivity (B-II.1) (Fig. 4). Many failure scars start at *ca* 500 to 650 m water depth, and connect to downslope erosional furrows (S-7) (Fig. 7). Slope failure scars are typically 1 km wide and involve a relatively small volume of sediment (range of a few km^3). Furrows are filled with fine unlithified sediments while furrow ridges that form a cemented surface are partly covered by cold-water corals. There, the mounds have a synoptic relief (up to 70 m above the surrounding sea floor) (Fig. 6C to E). The association of medium reflectivity (C-1), combined echo-facies (V-3) and along-slope linear erosive structures (S-5) characterizes the lower slope and basin. This area shows a large and weakly sinuous channel that extends about 20 km to the north (Fig. 8). It has a U-shape, is 4 km wide and 25 to 30 m deep (Fig. 8). This particular feature corresponds to a contourite moat defined by Faugères *et al.* (1999) as an erosional depression related to the presence and the intensity of a contour current on the sea bed (Principaud *et al.*, 2017). This domain mainly corresponds to fine-grained (i.e. wackestones) contourites deposited by contour currents flowing northward (Fig. 8) [Ocean Drilling Program (ODP) Site 626, Leg 101; Austin *et al.*, 1986].

South of Bimini Islands, the middle slope is incised over more than 100 km by narrow, elongated, sub-parallel, regularly spaced gullies with an average length of 4 km and an average spacing of 750 m. They are aligned perpendicularly between 410 m and 710 m water depth and are

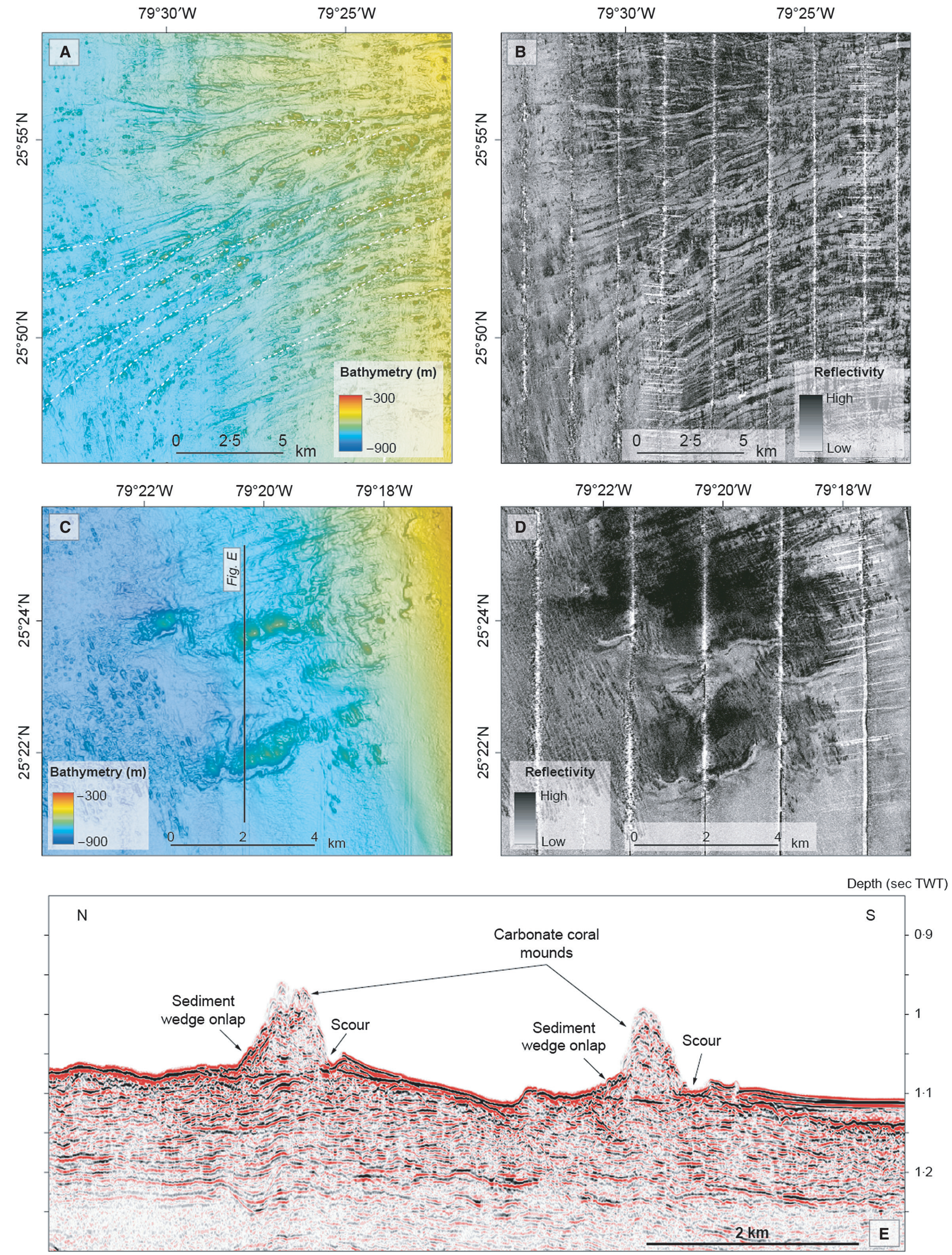

79°30′W
79°25′W
25°55′N
25°50′N
A
Bathymetry (m)
−300
−900
0 2·5 5 km
B
Reflectivity
High
Low
79°22′W
79°20′W
79°18′W
25°24′N
25°22′N
C
Fig. E
D
0 2 4 km
Depth (sec TWT)
N
S
Carbonate coral mounds
Sediment wedge onlap
Scour
0·9
1
1·1
1·2
2 km
E

Fig. 6. Physiography of the carbonate mounds areas along the western slope of the Great Bahama Bank. (A) Bathymetry; and (B) high resolution EM302 acoustic imagery maps showing the general distribution of carbonate mounds. They are often aligned obliquely to the general dip of Great Bahama Bank (GBB) slope, on the edges of the erosional furrows, indicated by white-dashed lines. (C) Bathymetry; (D) high resolution EM302 acoustic imagery maps of the highest carbonate mounds along the study area; and (E) multi-channel seismic profile across these two carbonate mounds.

predominantly straight with shallow incisions not exceeding 10 m in depth (Fig. 9A and B). In the southern area, at around 450 m water depth, a 40 m high escarpment dissects the slope, parallel to the platform edge, and extends over 40 km in this study's data set (Fig. 9C). The escarpment extends further south to a total length of 60 km and is interpreted as an incipient failure scar (Schnyder *et al.*, 2016). It forms a straight submarine cliff in the middle of the slope, and clearly cross-cuts the modern gullies, indicating a very young age of formation. On the middle slope, older large-scale escarpments form abrupt morphological cliffs with steep 25° gradients and heights of 80 to 100 m. Three prominent failure scarps can be clearly observed, extending over 9 km from south to north. Long spurs, which appear to be remnant of the original slope that has slid away, separate them (Fig. 10A and B) (Principaud *et al.*, 2015). The longest is 3·2 km long and *ca* 400 to 800 m wide and is covered by up to 5 m high cold-water coral mounds (Correa

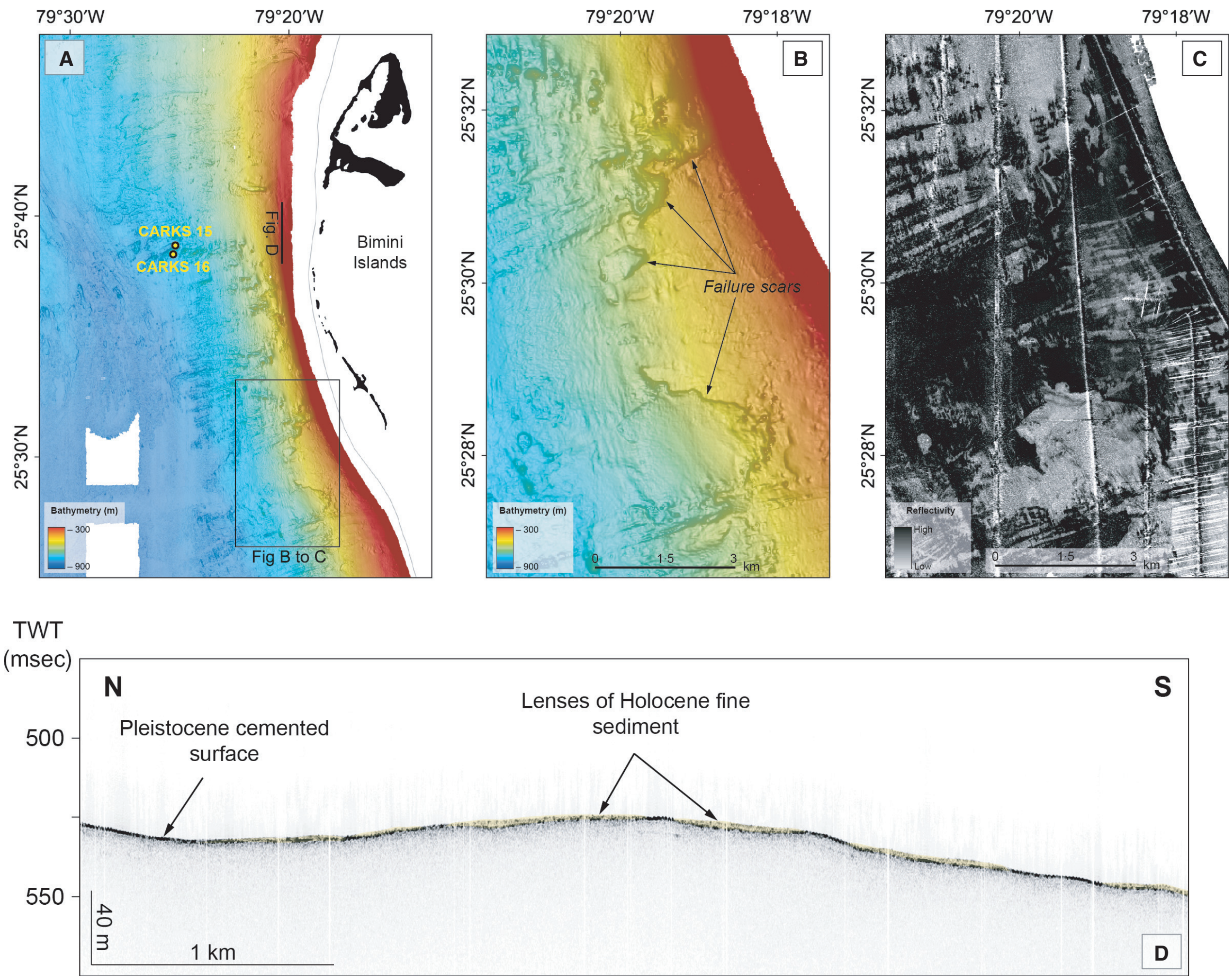

Fig. 7. (A) and (B) Bathymetric, and (C) high resolution EM302 acoustic imagery maps of the upper slope sea bed along the Bimini Islands area. (D) Chirp profile showing the physiography of the upper slope sea bed.

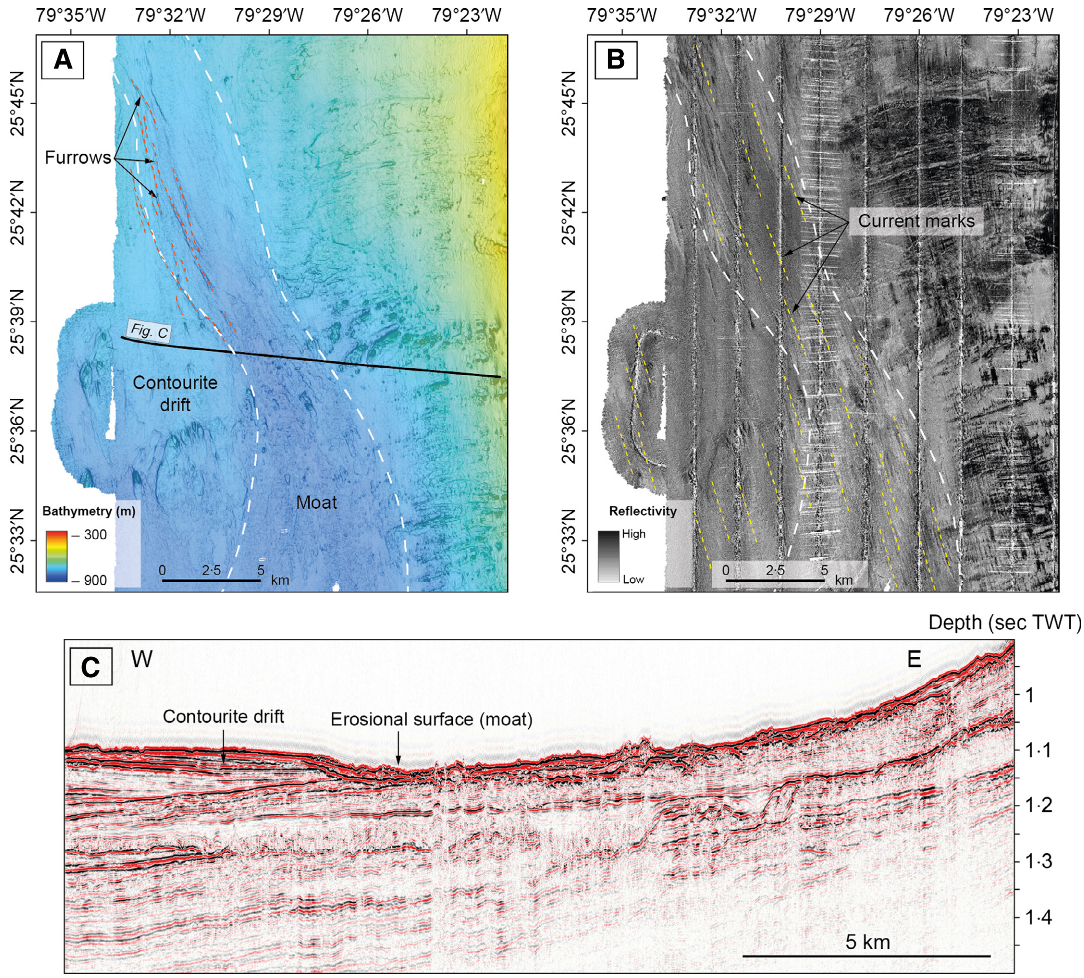

Fig. 8. Physiography of the contourite moat marked in the northern part of the study area. (A) EM302 map. (B) EM302 acoustic imagery map. (C) High resolution seismic profile.

et al., 2012b). Small, dispersed 50 m wide circular pockmarks are found at the top of the northern scar and are interpreted as fluid escape during the massive sediment collapse (Fig. 10B) (Principaud *et al.*, 2015). Sedimentary prisms border the toe of the scarps and adjacent spurs, displaying a flat to wavy surface overlain by sediment waves. The internal sides of the escarpments are underlain by 10 m deep moats. Locally, plunge pools developed (Fig. 10). This area is also affected by strong along-slope currents as indicated by the south–north lineaments, interpreted as scours and erosional marks located at the south of both debris blocks and carbonate mounds (Fig. 10A) (Grasmueck *et al.*, 2007; Correa *et al.*, 2012a,b). This set of spurs has been interpreted as the scars of large, multiphase MTC described in Principaud *et al.* (2015). The lower slope domain is characterized by an irregular surface (Fig. 10C) extending basinward over about 300 km^2 and a very low gradient of 0·2°. The MTC ends at 850 m water depth with large angular megablocks, 1 to 2 km wide and 50 m thick. The space between the blocks of the MTC is affected by bottom-current erosion (Fig. 10C). The hummocks and the megablocks form topographic highs, which provide a substrate for the growth of deep water coral communities (Grasmueck *et al.*, 2007; Correa *et al.*, 2012a,b; Fig. 10C).

Parameters controlling sediment export along the Great Bahama Bank slope

The strong export of sediments is highly controlled by GBB trade-wind-induced surface currents which act along the platform top and are responsible for the distribution of sediments and the prevailing off-bank transport to the western leeward side of the bank (Boardman & Neumann, 1984; Roth & Reijmer, 2004; Reijmer

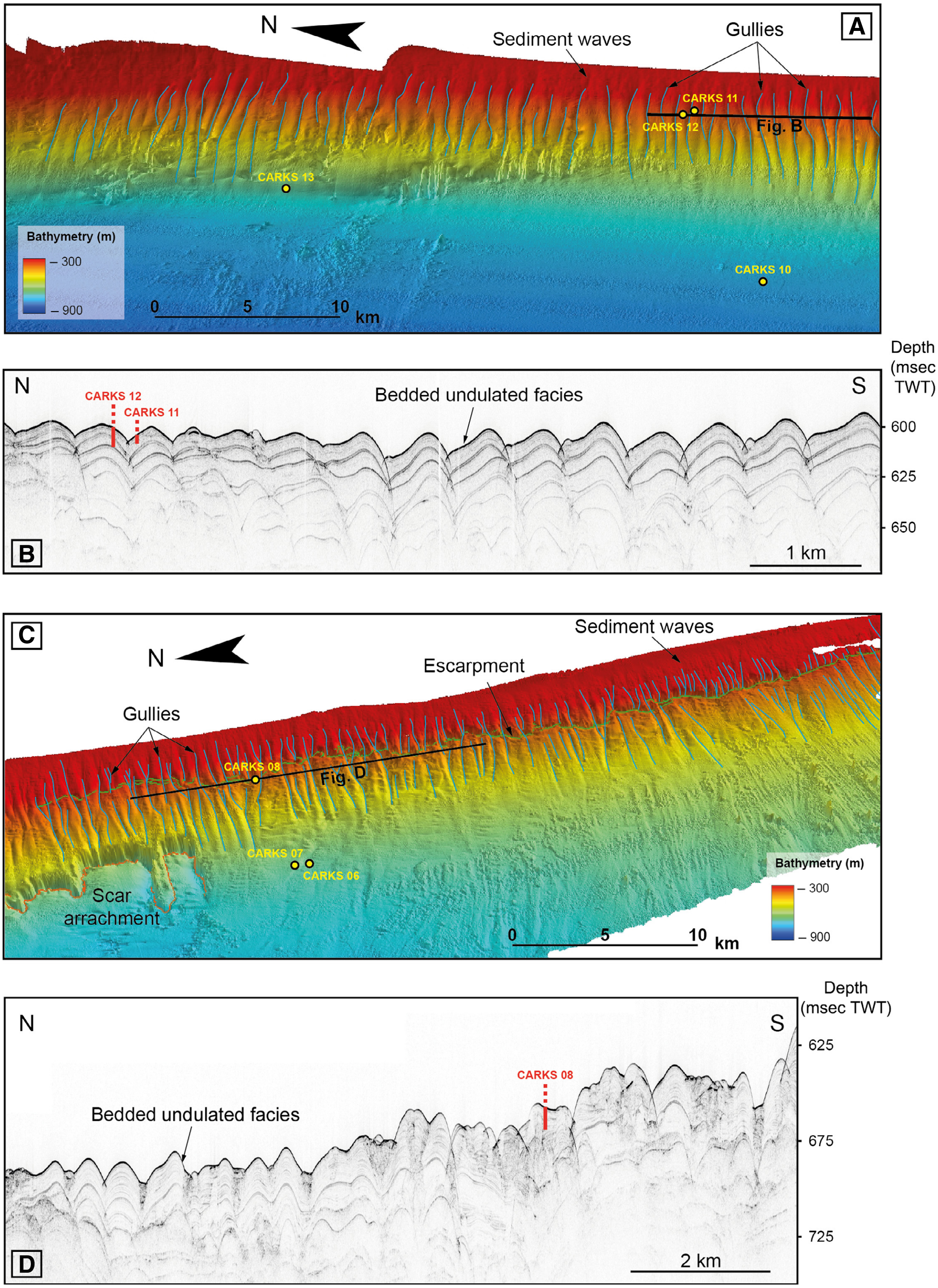

Fig. 9. Physiography of the gully system along the north-western Great Bahama Bank slope. (A) Bathymetric three-dimensional (3D) view of regular gullies. (B) Chirp profile across the regular gullies. (C) Bathymetric 3D view of irregular gullies. (D) Chirp profile across the irregular gullies.

et al., 2009; Purkis *et al.*, 2014). However, the morphological features present along the platform edge also influence the rate of off-bank transport. Pleistocene aeolianites and beach deposits which form a series of elongate rocky islands of Bimini and the ooid sand belt (Cat

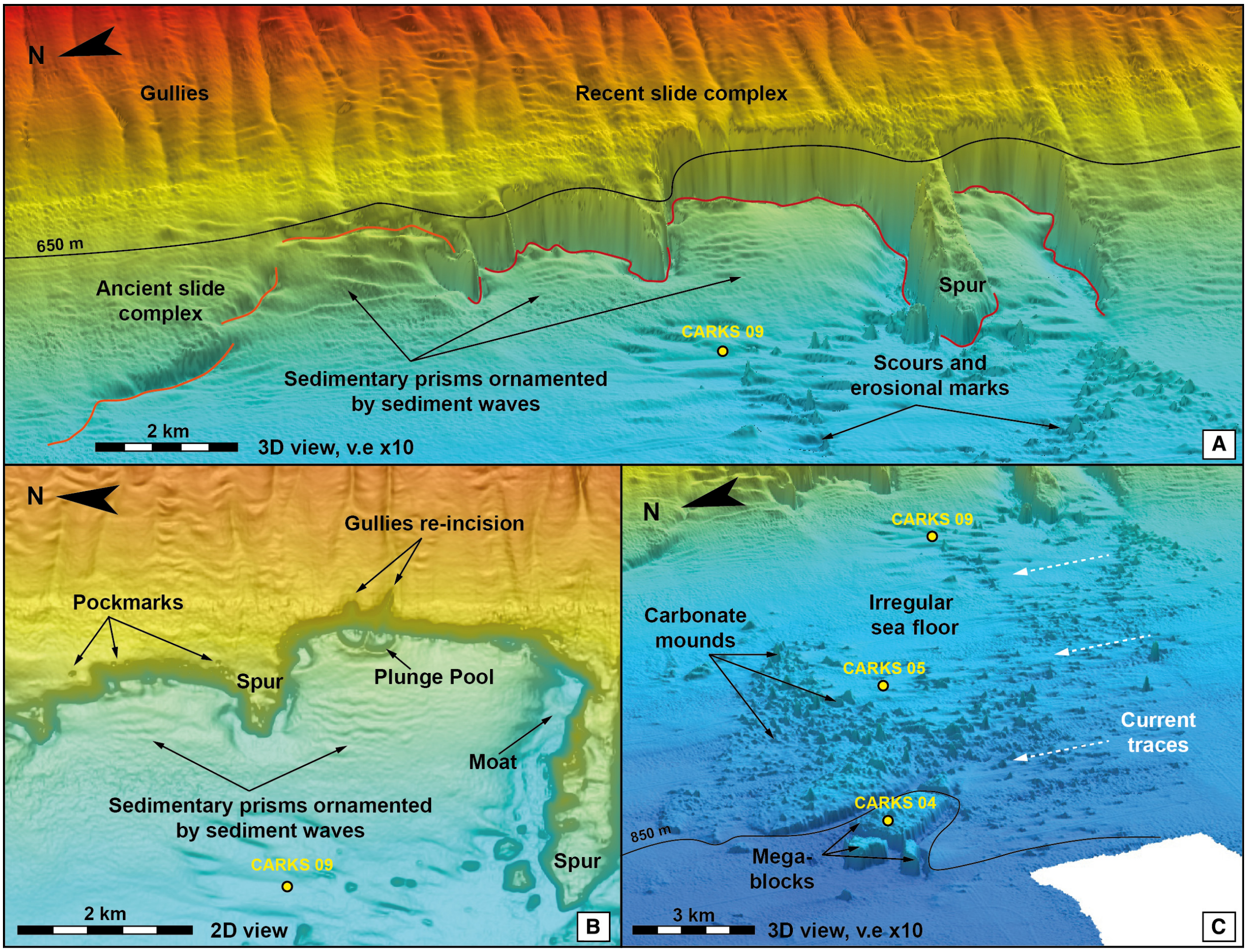

Fig. 10. Close-up views of the main morphological features constituting by the mass transport complex (MTC) with a vertical exaggeration of ×10. (A) The proximal zone shows steep outer walls to the south and an ancient slide complex to the north, infilled by a sedimentary prism overlain by sediment waves. (B) Close-up of the slide scar, which shows the location of the pockmarks at the top of the scar, the plunge pools vertically below the gully incisions, and the moat that follows the scarp. (C) The distal area, characterized by irregular sea floor morphology due to the mass transport, which ended in large megablocks.

Cay Shoal) constitute a 50 km continuous barrier along the margin (Fig. 1B). They were interpreted to have prevented off-bank transport of sediments from east to west during initial phases of bank flooding along the bank margin north of Ocean Cay (Figs 1 and 11; Gomes da Cruz, 2008). North and south of these obstacles, aragonitic mud-size particles from the platform are steadily exported and deposited on the upper to middle slope by daily tides and episodic cascading density flows. The change of sedimentation rates between these two domains could be linked to the presence or absence of gullies on the slope. In the south, sediment from the platform is exported and then transited through the gullies until reaching the lower slope by density cascading. Sedimentation rates are higher along the lower slope (40 to 50 cm ka^{-1}) than along the middle slope (15 to 30 cm ka^{-1}) during the Holocene (Fig. 11). In contrast, the north of Bimini Islands corresponds to a leeward extended slope (Mullins & Neumann, 1979; Hine *et al.*, 1981) without a gully system and with prevailing north-west winds. Sediments derived from the bank stay on the upper to middle slope and form a thick wedge that could explain the very high sedimentation rates.

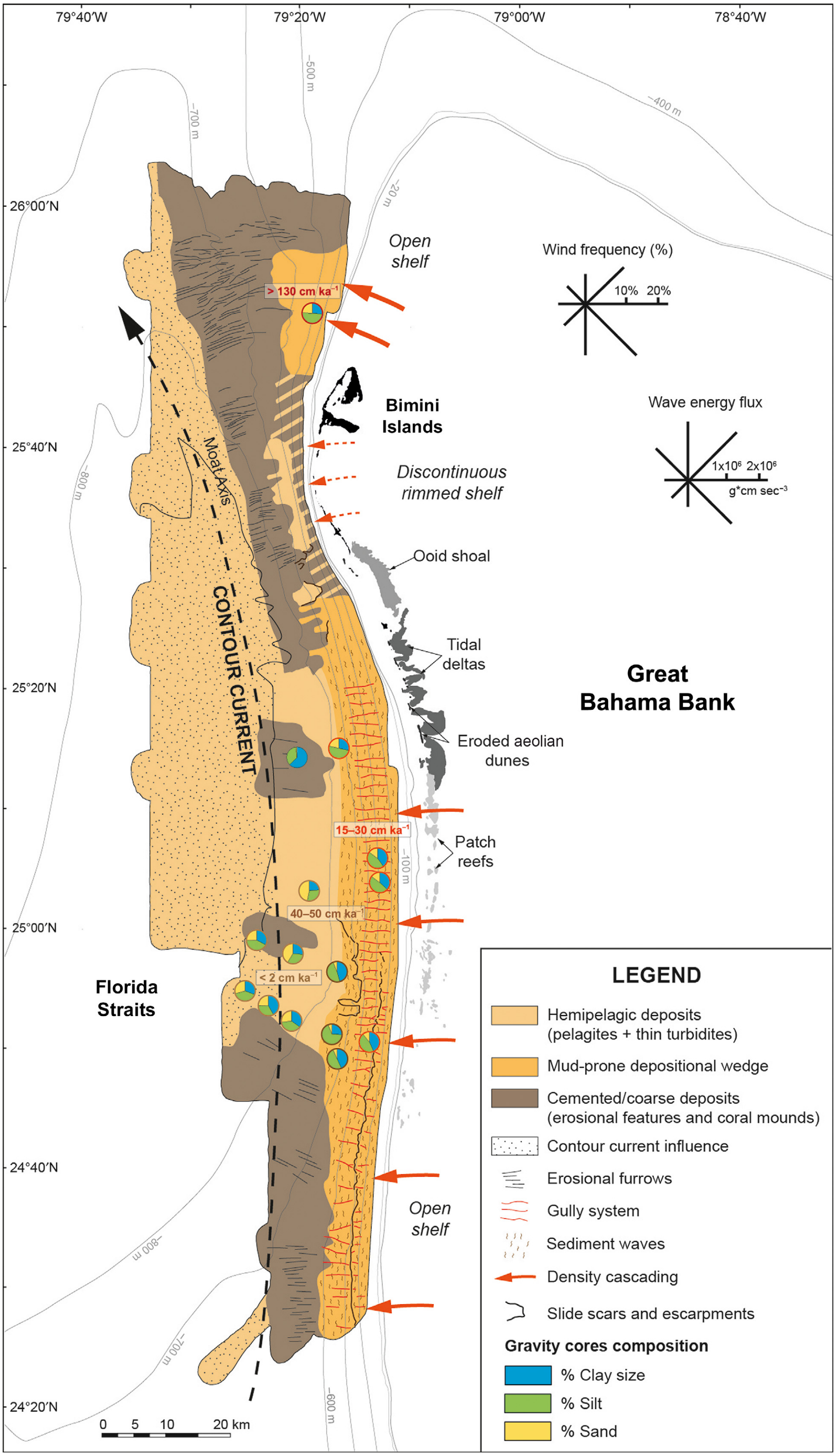

Fig. 11. Synthetic map of the recent sedimentary processes active over the north-western Great Bahama Bank slope and adjacent basin, determined by EM302 imagery and echo-character mapping. Position of the surface gravity cores indicating individual grain-size characteristics, and Holocene mean sedimentary rate along the slope.

© 2018 The Authors. Sedimentology © 2018 International Association of Sedimentologists,

Variation of hydrodynamic processes controlling the sedimentary distribution along the margin and relationship with Great Bahama Bank slope morphology

Density cascading and gully system

The daily tide and wind-driven surface currents export fine-grained material off of the bank that then settles from the water column at different slope depths (Heath & Mullins, 1984; Wilson & Roberts, 1995; Rendle-Bühring & Reijmer, 2005). This process is unlikely to produce erosion on the slope. However, fluids with large density contrast, either from sediment or higher salinity or a combination of both, cascading from the shallow waters of the platform to the basin have enough energy to erode the slope (Wilber *et al.*, 1990; Wilson & Roberts, 1992, 1995; Rendle & Reijmer, 2002; Betzler *et al.*, 2014). During the winter period, the Bahamas are regularly subjected to the influence of continental cold fronts coming from the Arctic that cause a rapid cooling of the platform waters (Fernandez-Partegas & Mooers, 1975; Wilson & Roberts, 1992). Combined with intense winds and wave action, it results in resuspension of large amounts of sediment that plunge into the basin. In summer, density currents are controlled by heat and moisture flux. High rates of evaporation increase the temperature and salinity of shallow waters thus causing dense water formation (Wilson & Roberts, 1995). This particular sedimentary process occurs throughout the year with variable frequencies and intensities, and provides a line source of sediment throughout the slope as indicated by the occurrence of a gully system and abundant sediment waves (Figs 11 and 12). Sediment waves located at the top of gullies represent the area where cascading flows become dense enough to reach the sea floor and deposit sediment. Sediment waves located deeper than the mouth of gullies are probably cyclic steps (Betzler *et al.*, 2014). These types of sediment waves form when a hydraulic jump occurs due to the change in slope angle, transforming the flow regime from supercritical to subcritical (Kostic, 2011). The greater sedimentary rates observed at the end of the gully system indicate a bypass sediment transfer on the upper to middle slope. Density cascading linked to off-bank transport was the major sedimentary process during highstand periods, when the platform is flooded (for example, 0 to 7·23 ka BP) (Boss & Rasmussen, 1995; Roth & Reijmer, 2004, 2005). The wedges along the northern Nicaragua Rise also occur during the late part of sea-level transgression and the highstand period following the flooding of bank and shelf tops (Glaser & Droxler, 1991). Indeed, the last part of the sea-level rise at each glacial termination coincides with the onset of aragonite production and off-bank transport (Jorry *et al.*, 2010). In contrast, during the exposure of the platform and the reduction of shallow-water, carbonate production causes the suspension of density cascading and the gully system (Fig. 12).

Slope instabilities and erosional features

Slope instabilities and erosional features are abundant on the present-day sea floor of the north-western slope of GBB. They are usually initiated along the middle slope and extend towards the basin for over 20 km. These slope instabilities are represented by variable shape failure scars and MTCs (Figs 11 and 12). Large MTCs on the present-day GBB slope correspond to successive mass gravity flow events that occurred during the Pliocene and Pleistocene (Principaud *et al.*, 2015). Repeated upslope failures impressive in size (several tens of kilometres long) have significantly affected the stratigraphic architecture at the lower slope and basin since the Miocene (Principaud *et al.*, 2015, 2017); they seem to be generated during eustatic falls after periods of very high rates of slope sedimentation (Principaud *et al.*, 2017). Westward of Bimini, the steep slopes, together with high sedimentation rate, may have locally caused upslope failure and triggered large collapse events. Submarine instabilities and sliding may be caused by decreasing sediment shear strength at parallel sea floor decollement planes, which commonly occur in mud deposits undergoing fluid-overpressure at the upper to mid-slope. Fluids may have been rapidly trapped as sedimentation rates upon the slope would have been high.

Early cementation can also be considered as a major preconditioning factor in MTC triggering. Principaud *et al.* (2015) showed that Plio-Pleistocene MTCs all glided along a common privileged decollement surface which coincided with a regional diagenetic key stratigraphic surface. In ODP Leg 166 wells, early cementation is characterized by well-lithified intervals (i.e. hardgrounds) which are found almost exclusively in glacial lowstand deposits and interpreted to have formed at or near the sea floor (Malone *et al.*, 2001). The lithified hardgrounds produce abrupt shifts in the index properties and shear

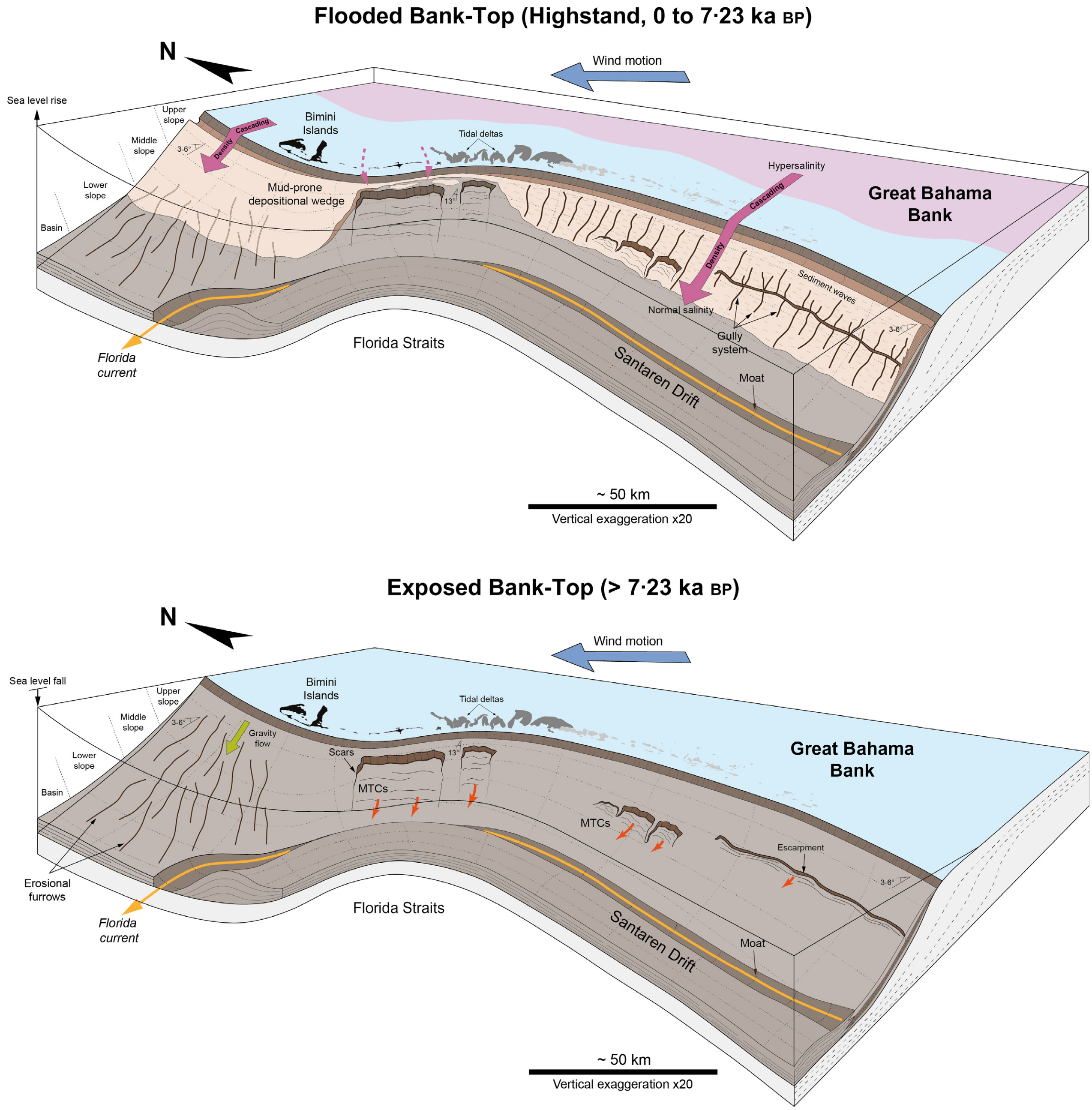

Fig. 12. Synthetic block diagram illustrating the different sedimentary processes identified along the north-western Great Bahama Bank slope during highstand and lowstand. This explains sedimentary transfer processes from the platform to the slope and the basin. MTC, mass transport complex.

strengths with unlithified to partially lithified portions. Just above the lithified intervals, slope failure may occur along a potentially weak detachment layer with a low shear strength. Although the slope is steeper in the first 300 m, most slope instabilities occur further downslope where slope angles are <2° to 3° (Principaud *et al.*, 2015; Tournador *et al.*, 2015). On the slopes of Little Bahama Bank a diagenetic front expressed by the transition from hardground and nodular facies coincides with the upper limit of the slope canyons (Tournadour, 2015). Such a downslope diagenetic front could produce an area with a weaker shear strength on the low-angle slope that results in intra-slope instability at *ca* 500 to 600 m water depth; or lower shear strength could be the result of high sedimentation rates at that depth of the GBB slopes (Eberli *et al.*, 1997). Older slope instabilities seem to coincide with Miocene and Pleistocene major sea-level falls after times of highest rates of slope sedimentation (Wunsch *et al.*, 2016; Principaud *et al.*, 2017).

Current regimes and carbonate mounds

Three current regimes influence the sediment distribution on the western slope of GBB: (i) downslope gravity currents; (ii) the oceanic Florida Current; and (iii) the internal tide that mostly affects the lower slope (Correa *et al.*, 2012a,b; Hebbeln *et al.*, 2012; Betzler *et al.*, 2014).

The downslope gravity currents are both cascading high-density currents either from high-salinity or sediment suspension, and other mass gravity flows including turbidites, debris flows and MTCs. They transport the sediments from bank-top to the adjacent slope and basin and have an erosional capacity that results in gullies, furrows and plunge pools at the base of erosional scars (Figs 9 and 10). Muds and fine sands from the platform interior are transported through density cascading (Wilson & Roberts, 1995) and/or turbidity currents to form a thick sediment wedge on the low-angled slopes during interglacials, whereas downslope mass gravity flows deliver the coarser fractions which are preferentially deposited at the toe of slope and in the basin (Rendle-Buehring & Reijmer, 2005). Most of the turbidite deposits are difficult to discriminate from hemipelagite while all of the exported material is fine-grained.

The Florida Current is a warm surface current with maximum current velocity in the top 200 m of water depth and only reaches the sea floor in the middle of the Straits and along the slope of GBB (Richardson *et al.*, 1969; Neumann & Ball, 1970; Wang & Mooers, 1997; Bergman, 2005). A current flowing through the Old Bahama Channel to the north has a confluence in the southern portion of the study area where the Straits of Florida and the Santaren Channel meet. Both Santaren and Florida currents feed the Santaren Drift (Anselmetti *et al.*, 2000). It was initiated during the Langhian, and evolved until the present day throughout successive phases of growth and lateral migration (Anselmetti *et al.*, 2000; Principaud *et al.*, 2017). Currently, the main depositional centre of the drift is the middle of the Santaren Channel. Between the drift and the slope a moat exists that is clearly visible in seismic and multi-beam bathymetry data (Fig. 8). In the moat the current winnows the fine-grained sediment (Eberli *et al.*, 1997; Rendle-Buehring & Reijmer, 2005) and produces current marks around carbonate mounds (Fig. 8) (Neumann & Ball, 1970; Betzler *et al.*, 2014; Lüdmann *et al.*, 2016). This winnowing is documented by grain-size data that show medium to coarse foraminiferal sand with a reduced percentage of mud-size particles beyond 800 m water depth (Table 4). The current-related winnowing and deposition interacts constantly with gravity flows, which interfinger with contourite deposits or become trapped and confined within the moat (Bergman, 2005; Principaud *et al.*, 2015, 2017).

In addition to the north-flowing Florida Current, an internal tide reverses its flow from north to south every 6 h along the base of the western slope of GBB (Correa *et al.*, 2012a). The current velocity reaches up to 0·5 m sec^{-1} measured through the 40 m water column above the sea floor with an autonomous underwater vehicle (AUV; Grasmueck *et al.*, 2007). This speed is a bit slower than the surface velocity (0·6 m sec^{-1}) of the Florida Current along the eastern side of the Straits of Florida; in the main axis the velocity of the Florida Current is 1·8 m sec^{-1}, three times as fast (Richardson *et al.*, 1969; Wang & Mooers, 1997; Bergman, 2005). The internal tide is generated by the reverberation of the surface tide on the steep slopes of the Bahamian platforms. It is also diurnal but is out of phase with the surface tide (Grasmueck *et al.*, 2007; Correa *et al.*, 2012a,b). North–south striation of fine sediment and backscatter data in the southern study area are likely to be caused by this current regime. Off Bimini, the backscatter striation does not follow this pattern (Grasmueck *et al.*, 2007). The reversing tide produces bidirectional cross-bedding in the pteropod rudstones of CARKS-16 (Sianipar, 2013).

Many studies have highlighted the correlation of ocean currents and the occurrence of cold-water carbonate mounds throughout the Florida Straits and the Santaren Channel off GBB (e.g. Mullins & Neumann, 1979; Mullins *et al.*, 1980, 1987; Bergman, 2005; Grasmueck *et al.*, 2007; Correa *et al.*, 2012a,b; Betzler *et al.*, 2014; Principaud *et al.*, 2015, 2017; Lüdmann *et al.*, 2016). Cold-water coral mounds occur in water depths between 250 m and 850 m along the western slope of GBB as single corals, in clusters and in mounds. Their distribution is strongly related to sedimentation rates, current regime and underlying topography (Correa *et al.*, 2012a,b; Lüdmann *et al.*, 2016). Boulders and blocks from the mass-wasting events are often overgrown by macroepibenthos and are the foundation for cold-water coral mounds (Correa *et al.*, 2012a,b; Hebbeln *et al.*, 2012; Lüdmann *et al.*, 2016). Elongated mounds are aligned with the direction of the bottom currents and form by the active growth of cold-water corals on elevated substrate with low sedimentation rate (Lüdmann *et al.*, 2016).

CONCLUSION

This study provides new valuable data on the morphology of Great Bahama Bank (GBB) slopes and interpretations of processes governing the sedimentary records. New high-quality acoustic data image the leeward margin of Great Bahama Bank and the adjacent floor of the Florida Straits in unprecedented detail and size. It shows the importance of inherited palaeotopography that lies below present-day sedimentary deposits and the complex interaction between gravity flow processes, oceanographic processes (density cascading) and contour currents.

The detailed study of the surface data reveal a downslope facies distribution characterized by large slope parallel longitudinal bands associated with specific morphological features that accurately depict the interplay of different sedimentary processes along the slope. Two major stratigraphic surfaces are superimposed and highlighted distinct sedimentary processes according to sea-level variations.

1 Slope instabilities and erosional features occur along the middle to lower slope during exposed top-bank (for example, >7·23 ka BP). These intra-slope gravity processes are characterized by lithified or coarse-grained deposits which form the antecedent irregular topography for the Holocene sedimentation.

2 A thinning-downslope sedimentary wedge generally associated with a gully system is present along most of the upper to middle slope. It consists of predominantly aragonite mud-size particles derived from the bank by density cascading processes occurring during periods of bank-top flooding (for example, 0 to 7·23 ka BP).

The along-slope variability of the Holocene wedge is linked to the presence of Bimini emerged islands and shoals which form a continuous barrier and block the off-bank sediment export. Conversely, areas that are open to the Straits show high sedimentation rates related to intense off-bank export.

Oceanic currents are responsible for the redistribution of the sediment along the slope. The effect of contour currents is most significant on the lower slope where it erodes and winnows muddy particles, which are deposited further along the slope or form a drift in the basin.

ACKNOWLEDGEMENTS

The authors would like to thank the captain and crew of the *R/V Le Suroît* for the quality of the data acquired and Ifremer-Genavir for the organization of the cruise and onboard data pre-processing. This work has been supported by the French INSU program “Actions Marges”. The first author was awarded a grant by the company Total through the Cifre program. G.P. Eberli acknowledges the support of the industrial associates of the CSL – Center for Carbonate Research. Careful reviews and constructive comments by Stephan Jorry, Xavier Janson, Elias Samankassou and Associate Editor John Reijmer, which helped to improve the manuscript, are gratefully acknowledged.

REFERENCES

Adams, E.W. and **Schlager, W.** (2000) Basic types of submarine slope curvature. *J. Sed. Res.*, **70**, 814–828.

Anselmetti, F.S., **Eberli, G.P.** and **Zan-Dong, D.** (2000) From the Great Bahama Bank into the Straits of Florida: a margin architecture controlled by sea level fluctuations and ocean currents. *Geol. Soc. Am. Bull.*, **112**, 829–846.

Atkinson, L.P., **Berger, T.**, **Hamilton, P.**, **Waddell, E.**, **Leaman, K.** and **Lee, T.N.** (1995) Current meter observations in the Old Bahama Channel. *J. Geophys. Res. Oceans*, **100**, 8555–8560.

Austin, J.A., **Schlager, W.** and **Cruise Participants** (1986) Proceedings of the Ocean Drilling Program, Initial Reports Vol. 101. College Station, Texas, (Ocean Drilling Program).

Ball, M.M. (1967) Carbonate sand bodies of Florida and the Bahamas. *J. Sed. Petrol.*, **37**, 556–591.

Bergman, K.L. (2005) Seismic analysis of paleocurrent features in the Florida Straits; insights into the paleo-Florida Current, upstream tectonics, and the Atlantic-Caribbean connection. Unpublished PhD Thesis, University of Miami, Coral Gables, FL, 206 pp.

Bergman, K.L., **Westphal, H.**, **Janson, X.**, **Poiriez, A.** and **Eberli, G.P.** (2010) Controlling parameters on facies geometries of the Bahamas, an isolated carbonate platform environment. In: *Carbonate Depositional Systems: Assessing Dimensions and Controlling Parameters – The Bahamas, Belize and Persian/Arabian Gulf* (Eds H. Westphal, B. Riegl and G.P. Eberli), pp. 5–80. Springer Verlag, Berlin, Germany.

Betzler, C., **Reijmer, J.J.G.**, **Bernet, K.**, **Eberli, G.P.** and **Anselmetti, F.S.** (1999) Sedimentary patterns and geometries of the Bahamian outer carbonate ramp (Miocene and lower Pliocene, Great Bahama Bank). *Sedimentology*, **46**, 1127–1145.

Betzler, C., **Lindhorst, S.**, **Eberli, G.P.**, **Lüdmann, T.**, **Möbius, J.**, **Ludwig, J.**, **Schutter, I.**, **Wunsch, M.**, **Reijmer, J.J.G.** and **Hübscher, C.** (2014) Periplatform drift: the combined result of contour current and off-bank transport along carbonate platforms. *Geology*, **42**, 871–874.

Boardman, M.R. and **Neumann, A.C.** (1984) Sources of periplatform carbonates: Northwest Providence Channel, Bahamas. *J. Sed. Petrol.*, **54**, 1110–1123.

Boss, S.K. and **Rasmussen, K.A.** (1995) Misuse of Fischer plots as sea-level curves. *Geology*, **23**, 221–224.

Carew, J.L. and **Mylroie, J.E.** (1997) Geology of the Bahamas. In: *Geology and Hydrogeology of Carbonate Islands, Developments in Sedimentology 54* (Eds H.L. Vacher and T.M. Quinn), pp. 91–139. Elsevier Science Ltd., Amsterdam, the Netherlands.

Chabaud, L. (2016) Modèle stratigraphique et processus sédimentaires au Quaternaire sur deux pentes carbonates des Bahamas (leeward et windward). Unpublished PhD Thesis, Université de Bordeaux, Bordeaux, France, 421 pp.

Chabaud, L., **Ducassou, E.**, **Tournadour, E.**, **Mulder, T.**, **Reijmer, J.**, **Conesa, G.**, **Giraudeau, J.**, **Hanquiez, V.**, **Borgomano, J.** and **Ross, L.** (2016) Sedimentary processes determining the modern carbonate periplatform drift of Little Bahama Bank. *Mar. Geol.*, **378**, 216–229.

Coniglio, M. and **Dix, G.R.** (1992) Carbonate slopes. In: *Facies Models: Response to Sea-level Change* (Eds R.G. Walter and N.P. James), GEOtext 1, pp. 349–374. Geological Association of Canada, St. John's, Canada.

Correa, T.B.S., **Eberli, G.P.**, **Grasmueck, M.**, **Reed, J.K.** and **Correa, A.M.S.** (2012a) Genesis and morphology of cold-water coral ridges in a unidirectional current regime. *Mar. Geol.*, **326–328**, 14–27.

Correa, T.B.S., **Grasmueck, M.**, **Eberli, G.P.**, **Reed, J.K.**, **Verwer, K.** and **Purkis, S.** (2012b) Variability of cold-water coral mounds in a high sediment input and tidal current regime, Straits of Florida. *Sedimentology*, **59**, 1278–1304.

Damuth, J.E. (1979) Migrating sediment waves created by turbidity currents in the northern South China Basin. *Geology*, **7**, 520–523.

Damuth, J.E. (1980) Use of high-frequency (3·5-12 kHz) echograms in the study of nearbottom sedimentation processes in the deep-sea: a review. *Mar. Geol.*, **38**, 51–75.

Damuth, J.E. (1994) Neogene gravity tectonics and depositional processes on the deep Niger Delta continental margin. *Mar. Petrol. Geol.*, **11**, 320–346.

Damuth, J.E. and **Hayes, D.E.** (1977) Echo character of the East Brazilian continental margin and its relationship to sedimentary processes. *Mar. Geol.*, **24**, 73–95.

Denny, W.M., III, **Austin, J.A.** and **Buffler, R.T.** (1994) Seismic stratigraphy and geologic history of Middle Cretaceous through Cenozoic rocks, Southern Straits of Florida. *AAPG Bull.*, **78**, 461–487.

Ducassou, E., **Chabaud, L.**, **Schmidt, S.** and **Mulder, T.** (2014) High resolution biostratigraphy of Holocene on cores from the Bahamian slopes. In: *STRATI 2013* (Eds R. Rocha, J. Pais, J.C. Kullbery and S. Finney), pp. 1293–1296. Springer Geology, Berlin, Germany.

Eberli, G.P. and **Ginsburg, R.N.** (1987) Segmentation and coalescence of Cenozoic carbonate platforms, northwestern Great Bahama Bank. *Geology*, **15**, 75–79.

Eberli, G.P. and **Ginsburg, R.N.** (1988) Aggrading and Prograding Infill of Buried Cenozoic Seaways, Northwestern Great Bahama Bank. In: *Atlas of Seismic Stratigraphy* (Ed. A.W. Bally), *AAPG Stud. Geol.*, **27**, 97–103.

Eberli, G.P. and **Ginsburg, R.N.** (1989) Cenozoic progradation of northwester Great Bahama Bank, a record of lateral platform growth and sea-level fluctuations. In: *Controls on Carbonate Platform and Basin Systems* (Eds P.D. Crevello, J.A. Wilson, J.F. Read and F.J. Sarg), *SEPM Spec. Publ.*, **44**, 339–351.

Eberli, G.P., **Swart, P.K.**, **Malone, M.J.** and Cruise Participants (1997) Proceedings of the Ocean Drilling Program, Initial Reports Vol. 166. College Station, Texas. (Ocean Drilling Program).

Eberli, G., **Anselmetti, F.S.**, **Betzler, C.**, **Van Konijnenburg, J.-H.** and **Bernoulli, D.** (2004) Carbonate platform to basin transition on seismic data and in outcrop – Great Bahama Bank and the Maiella platform margin, Italy. *AAPG Mem.*, **81**, 207–250.

Embley, R.W. (1976) New evidence for occurrence of debris flow deposits in the deep sea. *Geology*, **4**, 371–374.

Embley, R.W. (1980) The role of mass transport in the distribution and character of deep-ocean sediments with special reference to the North Atlantic. *Mar. Geol.*, **38**, 23–50.

Enos, P. (1974) Map of surface sediment facies of the Florida-Bahama Plateau. *Geological Society of America Map Series MC-5*, 4th edn.

Ericson, D.B. and **Wollin, G.** (1956) Micropaleontological and isotopic determinations of Pleistocene climates. *Micropaleontology*, **2**, 257–270.

Ericson, D.B., **Ewing, M.** and **Wollin, G.** (1961) Atlantic deep-sea sediment cores. *Geol. Soc. Am. Bull.*, **72**, 193–286.

Faugères, J.-C., **Stow, D.A.V.**, **Imbert, P.** and **Viana, A.R.** (1999) Seismic features diagnostic of contourite drifts. *Mar. Geol.*, **162**, 1–38.

Fernandez-Partegas, J. and **Mooers, C.N.K.** (1975) A subsynoptic study of winter cold fronts in Florida. *Monthly Weather Rev.*, **103**, 742–744.

Freile, D., **Milliman, J.D.** and **Hillis, L.** (1995) Leeward bank margin *Halimeda* meadows and draperies and their sedimentary importance on the western Great Bahama Bank slope. *Coral Reefs*, **14**, 27–33.

Ginsburg, R.N. (2001) The Bahamas Drilling Project: Background and acquisition of cores and logs. In: *Subsurface Geology of a Prograding Carbonate Platform Margin, Great Bahama Bank* (Ed. R.N.E. Ginsburg), *SEPM Spec. Publ.*, **70**, 3–13.

Glaser, K.S. and **Droxler, A.W.** (1991) High production and highstand shedding from deeply submerged carbonate banks, northern Nicaragua Rise. *J. Sed. Res.*, **61**, 128–142.

Gomes da Cruz, F.E.G. (2008) Processes, patterns and petrophysical heterogeneity of grainstone shoals at Ocean Cay, Western Great Bahama Bank. Unpublished PhD Thesis, University of Miami, Coral Gables, FL, 244 pp.

Grasmueck, M., **Eberli, G.P.**, **Correa, T.**, **Viggiano, D.A.**, **Luo, J.**, **Wyatt, G.J.**, **Wright, A.E.** and **Reed, J.K.** (2007) AUV-based environmental characterization of deep-water coral mounds in the Straits of Florida. *OTC*, **18510**, 1–11.

Hanquiez, V., **Mulder, T.**, **Lecroart, P.**, **Gonthier, E.**, **Marchès, E.** and **Voisset, M.** (2007) High resolution seafloor images in the Gulf of Cadiz, Iberian margin. *Mar. Geol.*, **246**, 42–59.

Harris, P.M.M., **Purkis, S.J.**, **Ellis, J.**, **Swart, P.K.** and **Reijmer, J.J.** (2015) Mapping bathymetry and depositional facies on Great Bahama Bank. *Sedimentology*, **62**, 566–589.

Heath, K.C. and **Mullins, H.T.** (1984) Open-ocean, off-bank transport of fine-grained carbonate sediment in the Northern Bahamas. *Geol. Soc. London. Spec. Publ.*, **15**, 199–208.

Hebbeln, D., **Wienberg, C.** and **Cruise Participants** (2012) *Report and Preliminary Result of R/V Maria S. Merian Cruise MSM20-4.* WACOM – West-Atlantic-Cold-water Coral Ecosystems: The West Side Story. Bridgetown – Freeport, 14 March – 7 April 2012. Berichte, MARUM – Zentrum fur Marine Umweltwissenschaften, Fachbereich Geowissenschaften, Universitat Bremen, No.290, 120 pp.

Hine, A.C. and **Neumann, A.C.** (1977) Shallow carbonate-bank-margin growth and structure, Little Bahama Bank, Bahamas. *AAPG Bull.*, **61**, 376–406.

Hine, A.C., **Wilder, R.J.**, **Bane, J.M.**, **Neumann, A.C.** and **Lorenson, K.R.** (1981) Offbank transport of carbonate sands along open, leeward bank margins: Northern Bahamas. *Mar. Geol.*, **42**, 327–348.

Isemer, H.J. and **Hasse, L.** (1985) *The Bunker Climate Atlas of the North Atlantic Ocean.* Springer Verlag, New York, 342 pp.

Jo, A., **Eberli, G.P.** and **Grasmueck, M.** (2015) Margin collapse and slope failure along southwestern Great Bahama Bank. *Sed. Geol.*, **317**, 43–52.

Jorry, S.J., **Droxler, A.W.** and **Francis, J.M.** (2010) Deepwater carbonate deposition in response to re-flooding of carbonate bank and atoll-tops at glacial terminations. *Quatern. Sci. Rev.*, **29**, 2010–2026.

Kenter, J.A.M., **Ginsburg, R.N.** and **Troelstra, S.R.** (2001) Sea-level-driven sedimentation patterns on the slope and margin. In *Subsurface Geology of a Prograding Carbonate Platform Margin, Great Bahama Bank: Results of the Bahamas Drilling Project*(Ed. R.N. Ginsburg), *SEPM Spec. Publ.*, **70**, 61–100.

Kostic, S. (2011) Modeling of submarine cyclic steps: controls on their formation, migration, and architecture. *Geosphere*, **7**, 294–304.

Ladd, J.W. and **Sheridan, R.E.** (1987) Seismic stratigraphy of the Bahamas. *AAPG Bull.*, **71**, 719–736.

Leaman, K.D., **Vertes, P.S.**, **Atkinson, L.P.**, **Lee, T.N.**, **Hamilton, P.** and **Waddell, E.** (1995) Transport, potential vorticity, and current/temperature structure across Northwest Providence and Santaren Channels and the Florida Current off Cay Sal Bank. *J. Geophys. Res.*, **100**, 8561–8569.

Lee, T.N., **Leaman, K.D.** and **Williams, E.** (1995) Florida Current meanders and gyre formation in the Straits of Florida. *J. Geophys. Res.*, **100**, 8607–8620.

Lüdmann, T., **Paulat, M.**, **Betzler, C.**, **Möbius, J.**, **Lindhorst, S.**, **Wunsch, M.** and **Eberli, G.P.** (2016) Carbonate mounds in the Santaren Channel, Bahamas: a current-dominated periplatform depositional regime. *Mar. Geol.*, **376**, 69–85.

Malone, M.J., **Slowey, N.C.** and **Henderson, G.M.** (2001) Early diagenesis of shallow-water periplatform carbonate sediments, leeward margin, Great Bahama Bank (Ocean Drilling Program Leg 166). *Geol. Soc. Am. Bull.*, **113**, 881–894.

Masaferro, J.L. and **Eberli, G.P.** (1999) Chapter 7 Jurassic-Cenozoic structural evolution of the southern Great Bahama Bank. In: *Sedimentary Basins of the World* (Ed. P. Mann), pp. 167–193. Elsevier Science Ltd., Amsterdam, the Netherlands.

Masaferro, J.L., **Bulnes, M.**, **Poblet, J.** and **Eberli, G.P.** (2002) Episodic folding inferred from syntectonic carbonate sedimentation; the Santaren Anticline, Bahamas Foreland. *Sed. Geol.*, **146**, 11–24.

Milliman, J.D., **Freile, D.**, **Steinen, R.P.** and **Wilber, R.J.** (1993) Great Bahama Bank aragonite muds: mostly inorganically precipitated, mostly exported. *J. Sed. Petrol.*, **63**, 589–595.

Mulder, T., **Ducassou, E.**, **Eberli, G.P.**, **Hanquiez, V.**, **Gonthier, E.**, **Kindler, P.**, **Principaud, M.**, **Fournier, F.**, **Léonide, P.**, **Billeaud, I.**, **Marsset, B.**, **Reijmer, J.J.G.**, **Bondu, C.**, **Joussiaume, R.** and **Pakiades, M.** (2012) New insights into the morphology and sedimentary processes along the western slope of Great Bahama Bank. *Geology*, **40**, 603–606.

Mulder, T., **Ducassou, E.**, **Gillet, H.**, **Hanquiez, V.**, **Principaud, M.**, **Chabaud, L.**, **Eberli, G.P.**, **Kindler, P.**, **Billeaud, I.**, **Gonthier, E.**, **Fournier, F.**, **Léonide, P.** and **Borgomano, J.** (2014) First Discovery of Channel-Levee Complexes In A Modern Deep-Water Carbonate Slope Environment. *J. Sediment. Res.*, **84**, 1139–1146.

Mulder, T., **Joumes, M.**, **Hanquiez, V.**, **Gillet, H.**, **Reijmer, J.J.G.**, **Tournadour, E.**, **Chabaud, L.**, **Principaud, M.**, **Schnyder, J.S.D.**, **Borgomano, J.**, **Fauquembergue, K.**, **Ducassou, E.** and **Busson, J.** (2017) Carbonate slope morphology revealing sediment transfer from bank-to-slope (Little Bahama Bank, Bahamas). *Mar. Petrol. Geol.*, **83**, 26–34.

Mullins, H.T. and **Neumann, A.C.** (1979) Deep carbonate bank margin structure and sedimentation in the Northern Bahamas. In: *Geology of Continental Slopes* (Eds L.J. Doyle and O. H Pilkey), *SEPM Spec. Publ.*, **27**, 165–192.

Mullins, H.T., **Neumann, A.C.**, **Wilber, R.J.**, **Hine, A.C.** and **Chinburg, S.J.** (1980) Carbonate sediment drifts in the northern Straits of Florida. *AAPG Bull.*, **64**, 1701–1717.

Mullins, H.T., **Heath, K.C.**, **Van Buren, H.M.** and **Newton, C.R.** (1984) Anatomy of a modern open-ocean carbonate slope: northern Little Bahama Bank. *Sedimentology*, **31**, 141–168.

Mullins, H.T., **Gardulski, A.F.**, **Wise, S.W.** and **Applegate, J.** (1987) Middle Miocene oceanographic event in the eastern Gulf of Mexico: Implications for seismic stratigraphic succession and Loop Current/Gulf Stream circulation. *Geol. Soc. Am. Bull.*, **98**, 702–713.

Neumann, A.C. and **Ball, M.M.** (1970) Submersible observations in the Straits of Florida: geology and bottom currents. *Geol. Soc. Am. Bull.*, **81**, 2861–2874.

Principaud, M. (2015) Morphologie, architecture et dynamique sédimentaire d'une pente carbonatée moderne: Le *Great Bahama Bank* (Bahamas). Unpublished PhD Thesis, Université de Bordeaux, Bordeaux, France, 293 pp.

Principaud, M., **Ponte, J.-P.**, **Mulder, T.**, **Gillet, H.**, **Robin, C.** and **Borgomano, J.** (2017) Slope-to-basin stratigraphic evolution of the carbonate northwestern Great Bahama Bank (Bahamas) during the Neogene to Quaternary: Interactions between downslope and bottom currents deposits. *Basin Res.*, **29**, 699–724.

Purdy, E.G. (1963a) Recent calcium carbonate facies of the Great Bahama Bank: 1. Petrography and reaction groups. *J. Geol.*, **71**, 334–355.

Purdy, E.G. (1963b) Recent calcium carbonate facies of the Great Bahama Bank: 2. Sedimentary facies. *J. Geol.*, **71**, 472–497.

Purkis, S., **Kerr, J.**, **Dempsey, A.**, **Calhoun, A.**, **Metsamaa, L.**, **Riegl, B.**, **Kourafalou, V.**, **Bruckner, A.** and **Renaud, P.** (2014) Large-scale carbonate platform development of Cay Sal Bank, Bahamas, and implications for associated reef geomorphology. *Geomorphology*, **222**, 25–38.

Rankey, E.C. and **Doolittle, D.F.** (2012) Geomorphology of carbonate platform-marginal uppermost slopes: insights from a Holocene analogue, Little Bahama Bank, Bahamas. *Sedimentology*, **59**, 2146–2171.

Rankey, E.C. and **Reeder, S.L.** (2010) Controls on platform-scale patterns of surface sediments, shallow Holocene platforms, Bahamas. *Sedimentology*, **57**, 1545–1565.

Rankey, E.C. and **Reeder, S.L.** (2011) Holocene oolitic marine sand complexes of the Bahamas. *J. Sed. Res.*, **81**, 97–117.

Reijmer, J.J.G., **Swart, P.K.**, **Bauch, T.**, **Otto, R.**, **Reuning, L.**, **Roth, S.** and **Zechel, S.** (2009) A re-evaluation of facies on Great Bahama Bank I: new facies maps of Western Great Bahama Bank. Perspectives in Carbonate Geology: a Tribute to the Career of Robert Nathan Ginsburg. *Int. Assoc. Sedimentol. Spec. Publ.*, **98**, 29–46.

Rendle, R.H. and **Reijmer, J.J.G.** (2002) Quaternary slope development of the western, leeward margin of the Great Bahama Bank. *Mar. Geol.*, **185**, 143–164.

Rendle-Buehring, R.H. and **Reijmer, J.J.G.** (2005) Controls on grain-size patterns in periplatform carbonates: marginal setting versus glacio-eustacy. *Sed. Geol.*, **175**, 99–113.

Richardson, W.S., **Schmitz, W.J., Jr** and **Niiler, P.P.** (1969) The velocity structure of the Florida Current from the Straits of Florida to Cape Fear. *Deep-Sea Res.*, **16**, 225–231.

Roberts, H.H., **Rouse, L.J., Jr**, **Walker, N.D.** and **Hudson, J.H.** (1982) Cold-water stress in Florida Bay and northern Bahamas – a product of winter cold-air outbreaks. *J. Sed. Petrol.*, **52**, 145–155.

Roth, S. and **Reijmer, J.J.G.** (2004) Holocene Atlantic climate variations deduced from carbonate periplatform sediments (leeward margin, Great Bahama Bank). *Paleoceanography*, **19**, PA1003.

Roth, S. and **Reijmer, J.J.G.** (2005) Holocene millennial to centennial carbonate cyclicity recorded in slope sediments of the Great Bahama Bank and its climatic implications. *Sedimentology*, **52**, 161–181.

Schlager, W. and **Ginsburg, R.N.** (1981) Bahama carbonate platform - the deep and the past. *Mar. Geol.*, **44**, 1–24.

Schlager, W., **Reijmer, J.J.G.** and **Droxler, A.W.** (1994) Highstand shedding of carbonate platforms. *J. Sed. Res.*, **B64**, 270–281.

Schnyder, J.S.D., **Eberli, G.P.**, **Kirby, J.T.**, **Shi, F.**, **Tehranirad, B.**, **Mulder, T.**, **Ducassou, E.**, **Hebbeln, D.** and **Wintersteller, P.** (2016) Tsunamis caused by submarine slope failures along western Great Bahama Bank. *Sci. Rep.*, **6**, 35925.

Sealey, N.E. (1994) *Bahamian Landscapes: An Introduction to the Physical Geography of the Bahamas*. Media Pub., Nassau, Bahamas, 128 pp.

Shinn, E.A., **Steinen, R.P.**, **Lidz, B.H.** and **Swart, P.K.** (1989) Whitings, a sedimentologic dilemma. *J. Sed. Petrol.*, **59**, 147–161.

Sianipar, R.E. (2013) Composition of a cold-water coral mound “Matterhorn” and its surrounding sediments in the Straits of Florida. Unpublished MSc Thesis, University of Miami, Coral Gables, FL, 175 pp.

Swart, P.K., **Eberli, G.P.**, **Malone, M.J.** and **Sarg, J.K.** (2000) Proceedings of the ODP, Scientific Results 166. College Station, TX (Ocean Drilling Program).

Swart, P.K., **Reijmer, J.J.G.** and **Otto, R.** (2009) A re-evaluation of facies on Great Bahama Bank II: variations in the δ13C, δ18O and mineralogy of surface sediments. Perspectives in Carbonate Geology: a Tribute to the Career of Robert Nathan Ginsburg. *Int. Assoc. Sedimentol. Spec. Publ.*, **41**, 47–59.

Swart, P.K., **Oehlert, A.M.**, **Mackenzie, G.J.**, **Eberli, G.P.** and **Reijmer, J.J.G.** (2014) The fertilization of the Bahamas by Saharan dust: a trigger for carbonate precipitation? *Geology*, **42**, 671–674.

Tournador, E., **Mulder, T.**, **Borgomano, J.**, **Hanquiez., V.**, **Ducassou, E.** and **Gillet., H.** (2015) Origin and architecture of a mass transport complex on the northwest slope of Little Bahama Bank (Bahamas): relations between off-bank transport, bottom current sedimentation and submarine landslides. *Sed. Geol.*, **317**, 9–26.

Tournadour, E. (2015) Architecture et dynamique sédimentaire d’une pente carbonatée moderne : exemple de la pente nord de *Little Bahama Bank* (LBB), Bahamas. Unpublished PhD Thesis, Université de Bordeaux, Bordeaux, France, 348 pp.

Traverse, A. and **Ginsburg, R.N.** (1966) Palynology of the surface sediments of Great Bahama Bank, as related to water movement and sedimentation. *Mar. Geol.*, **4**, 417–459.

Unterseh, S. (1999) Cartographie et Caractérisation du Fond Marin par Sondeur Multifaisceaux. Unpublished PhD Thesis, Institut National Polytechnique de Lorraine, France, 234 pp.

Wang, J. and **Mooers, C.N.K.** (1997) Three-dimensional perspectives of the Florida current: transport, potential vorticity, and related dynamical properties. *Dynam. Atmosph. Oceans*, **27**, 135–149.

Wilber, R.J., **Milliman, J.D.** and **Halley, R.B.** (1990) Accumulation of bank-top sediment on the western slope of Great Bahama Bank: rapid progradation of a carbonate megabank. *Geology*, **18**, 970–974.

Wilber, R.J., **Whitehead, J.**, **Halley, R.B.**, **Milliman, J.D.**, **Wilson, P.A.** and **Roberts, H.H.** (1993) Carbonate-periplatforrn sedimentation by density flows: a mechanism for rapid off-bank and vertical transport of shallow-water fines: comment and Reply. *Geology*, **21**, 667–669.

Wilson, P.A. and **Roberts, H.H.** (1992) Carbonate-periplatform sedimentation by density flows: a mechanism for rapid off-bank and vertical transport of shallow-water fines. *Geology*, **20**, 713–716.

Wilson, P.A. and **Roberts, H.H.** (1995) Density cascading; off-shelf sediment transport, evidence and implications, Bahama Banks. *J. Sed. Res.*, **65**, 45–56.

Wunsch, M., **Betzler, C.**, **Lindhorst, S.**, **Lüdmann, T.** and **Eberli, G.P.** (2016) Sedimentary dynamics along carbonate slopes (Bahamas archipelago). *Sedimentology*, **64**, 631–657.

Manuscript received 26 February 2017; revision accepted 18 January 2018